Inhibition of HIV-1 immune modulation by small molecules targeting viral Nef- host CD80 interface

Anusmrithi U. Sharma[1,3], Shweta Sharma[4,5], Gandhimathi Arumugam[2], Archana Padmanabhan Nair[3], Srinivas Ambala[4,5], Gurunadham Munagala[4,5], Kushalava Reddy Yempalla[4,5], Akankshi Munjal[2], Shreenidhi Rajkumar[1], Neelagandan Kamariah[1], Ashok R. Venkitaraman[1,6], Ramanathan Sowdhamini[2], Taslimarif Saiyed[3], Parvinder Pal Singh[4,5]*, Ram A. Vishwakarma[3,5]*, Satyajit Mayor[2]*# and Anandi S. Karumbati[1,3]*

[1]Centre for Chemical biology and Therapeutics, Institute of Stem Cell Science and Regenerative Medicine, GKVK, Bellary Road, Bangalore, India

[2]National Centre for Biological Sciences, GKVK Campus, Bellary Road, Bangalore, India

[3]Centre for Cellular and Molecular Platforms, GKVK Campus, Bellary Road, Bangalore, India.

[4]CSIR-Indian Institute of Integrative Medicine, Canal Road, Jammu-180001, India.

[5]Academy of Scientific and Innovative Research (AcSIR), Ghaziabad-201 002, India.

[6]The Cancer Science Institute of Singapore, Centre for Translational Medicine, National University of Singapore, Singapore 117599 & Agency for Science, Technology and Research (A*STAR), 8A Biomedical Grove, Singapore 138648.

* Co-corresponding authors

Further information and requests for resources and reagents should be directed to and will be fulfilled by the lead contact, Satyajit Mayor (mayor@ncbs.res.in)

Abbreviations

Nef (Negative Regulatory Factor)

MHC (Major Histocompatibility Complex)

CD80/86 (Cluster of Differentiation 80 and 86)

APC (Antigen Presenting Cells)

AP (Aminopyrimidine)

PA (Phenoxyacetamide)

BC (Biaryl (heteroaryl) carbamate)

ART (antiretroviral therapy)

NNRTI (non-nucleoside inhibitors)

HAART (Highly Active Anti-Retroviral Therapy)

BnAb (Broadly neutralizing antibodies antibody)

LTNPs (Long-Term Non-Progressors)

MST (Micro-Scale Thermophoresis)

WST-1 (Water Soluble Tetrazolium-1)

SAXS (Small Angle X-ray scattering)

Keywords

immune modulation

HIV-1

Co stimulatory receptors- CD80/86

T-cell activation

Summary

HIV-1 causes diverse immunomodulatory responses in the host, including the down-regulation of co-stimulatory proteins CD80/86, mediated by HIV-1 protein Nef, blunting T-cell activation. Using a screening cascade of biochemical and cell-based assays, we identified potent small molecules representing three chemical scaffolds namely amino pyrimidine, phenoxy acetamide and bi-aryl heteroaryl carbamate which target the protein-protein interaction interface of CD80/86 and Nef with sub-micromolar potency. These molecules restore CD80/86 surface levels in HIV-1-Nef infected antigen presenting cells and T-cell activation. Nef-CD80 interface and small molecule binding sites were mapped by using computational docking and structural studies, followed by validation by mutational analysis. This analysis resulted in the identification of two key residues, K99 and R111, which were associated with down-modulation of CD80 surface levels by Nef and important for small molecule binding. Targeting these interacting residues disabled Nef-mediated down-modulation of CD80 surface levels, consequently restoring T-cell activation. Thus, we validate a new target, the Nef-CD80/86 protein-protein interaction interface, with a potential to develop new inhibitors to counteract the immunomodulatory consequences of HIV-1.

Introduction

1   Over the past decade, there has been tremendous effort in finding newer therapies

2   for HIV/AIDS. Increased use of anti-retroviral drugs has been accompanied by the

3   steady increase in HIV drug resistance and viremia that often result in

4   immunosuppression leading to morbidity[3]. Drug resistance is mainly transmitted at

5   the time of infection or acquired during previous treatment for instance in women

6   given anti-retroviral drugs to prevent mother-to-child transmission of HIV[4]. Other

7   treatment strategies like using anti-HIV-1 antibodies (bnAbs) are reported in

8   combination with ART which have the capacity to impact on HIV-1-specific T cell

9   immune responses in infected humans but whether it controls the virus remains to be

10 determined[5]. In addition, with the vaccine trials failing to elicit broad plasma

11 neutralization of primary virus isolates[6], there is an urgent need to fast-track the

12 transition to newer antiviral drug regimens which needs to be administered in multi-

13 drug combinations in order to combat the ever-evolving virus. Increasing drug

14 resistance also emphasizes the requirement of new molecules that can target the

15 host-viral interface with high specificity[7,8].

16 To obtain targets for the next generation of HIV-1 therapy we explored the interaction

17 interface of the essential HIV-1 accessory protein, Nef[9], with host proteins. Nef is a

18 27-35 kDa protein expressed during early phases of viral replication and helps

19 maintain a constant state of infection by disrupting T-cell activation, thereby allowing

20 evasion of the host immune system[10,11,12]. Evidence supporting a direct role for Nef

21 in HIV disease comes from transgenic mouse models developed, in which a CD4-

22 derived promoter was used to express Nef in various tissues including thymus,

23 kidney and lungs which progressed into AIDS-like phenotype, featuring CD4+ T-cell

24 loss, thymic involution, splenic atrophy and subsequent kidney and lung pathology[13].

1

25   This phenotype in many aspects' mimics human AIDS. Also in patient populations,

26   fortuitous deletions in the *nef* gene in HIV infected patients of the Sydney Blood

27   Bank Cohort remain essentially free of AIDS related symptoms[14,15]. In another study,

28   the proportion o*f nef* gene defects was found to be significantly higher in Long-Term

29   Non-Progressors (LTNPs) compared to progressors [16,17,18]. These animal and

30   patient studies suggests that Nef plays a pivotal role in pathogenesis and AIDS-like

31   progression in HIV-infected individuals[19].

32   Nef functions by re-engineering the levels of many surface proteins such as MHC-I,

33   CD4, CD28, CXCR4, and CD3 in infected cells, and redirecting them to

34   endosomes[20,21]. Nef interacts either directly or indirectly with multiple host partners

35   and functions to increase the pathogenesis of the virus[22,23]. Our previous work has

36   highlighted interactions of Nef with the host cell surface co-stimulatory proteins CD80

37   and CD86[24,25]. Down-regulation of CD80/86 is sufficient to cause impaired naïve T-

38   cell stimulation *in vitro* and *in vivo*[26]. We have shown that by administering just the

39   cytoplasmic tails of CD80 and CD86 in Nef-expressing cells, CD80/86 down

40   modulation is prevented, making this host-viral interface amenable for developing

41   new chemical biological tools and providing targets for therapeutic intervention.

42   The variety of functions carried out by Nef is based on its ability to interact with

43   multiple cellular proteins. This is possibly due to its structure; it has many flexible

44   regions, a feature unusual for cytoplasmic proteins. The unstructured regions of Nef

45   may ease the allosteric adjustments required for interaction of Nef with different

46   proteins. However, the flexible and unstructured features of Nef protein add

47   substantial challenges to structurally characterize the full-length Nef protein and

48   study their binding sites.

1

49   In the current study, we show that Nef directly binds to cytoplasmic tail peptides of

50   CD80 and CD86. We have identified small molecules, which can abrogate Nef

51   interactions with CD80 and/or CD86. The compounds mainly belong to 3 scaffolds

52   amino pyrimidine (**AP**), phenoxy acetamide (**PA**) and bi-aryl heteroaryl carbamate

53   (**BC**) having nanomolar to micromolar inhibition potencies *in vitro*. Representative

54   actives from these scaffolds were then validated in functional cell-based assays for

55   reverting the down regulation of cell surface Nef-mediated co-stimulatory protein

56   expression and re-establishing T-cell activation. These identified actives also

57   reversed similar Nef-mediated effects after viral infections.

58   To further improve the efficacy of these leads, we used an *in-silico* approach to

59   explore the binding mode of Nef with the co-stimulatory molecules. Full length Nef

60   protein was modeled and potential binding sites for CD80 were identified. Based on

61   these predictions a selected subset of CD80 interacting residues in Nef were

62   mutated and the corresponding mutants were examined in assay platforms to

63   confirm the model and its functional consequences. The understanding of the

64   druggable pocket opens the scope for future lead optimization work. Altogether, we

65   report a chemical strategy to inhibit Nef-mediated immunomodulatory functions,

66   which prevents immune evasion of HIV-infected cells. While these molecules may be

67   developed for future therapeutic intervention, at the current stage, they may be used

68   as chemical biology tools to understand the role of host-pathogen interface in the

69   form of Nef-CD80/86 interaction surface in HIV immune evasion.

70

71   **Results**

72   **Identification of potent Inhibitors that disrupt Nef-CD80/CD86 Interaction**

73   In our previous work, we have shown that cytoplasmic tail peptides from CD80 and

74   CD86 compete with the down modulation of surface CD80/86 by Nef protein in cell

75   based assays[25]. For our assays we have used Nef F2 recombinant protein of

76   Subtype-C origin (the alignment of the Nef sequence from this subtype with the

77   commonly used subtype B is presented in **Sup. Fig. S1a**). To ascertain direct

78   binding of Nef to the cytoplasmic tail peptide of the co-stimulatory receptors CD80 or

79   CD86 in microscale thermophoresis (MST) assay[27], we added 20-mer peptide of

80   CD80 or CD86 (**Fig. 1a, Sup. Fig. S1b**) to fluorescently labelled Nef. A 16-point

81   titration of peptides against Nef was carried out (see details in Star Methods). Nef-

82   CD80 interaction showed a saturation curve with a kD of 27 µM (**Fig.1b**). Nef-CD86

83   interaction showed a sigmoidal curve with 112 nM kD, indicating a higher affinity

84   interaction (**Fig.1c**). Having verified the direct binding of the CD80 and CD86

85   peptides with Nef in MST, we immobilized CD80/86 cytosolic peptides in a microtiter

86   plate and examined the binding of Nef in an ELISA assay (Scheme, **Sup. Fig. S1c**).

87   There was a 4-fold increase in the fluorescent signal due to binding of Nef to the 20-

88   mer CD80/86 cytosolic tail peptides compared to wells with an unrelated peptide

89   (from CD74), or with no peptide controls (**Fig. 1d**). We used this ELISA format to

90   screen and identify inhibitors of Nef-CD80 and Nef-CD86 interaction.

91   Small molecules were hand-picked for screening based on their drug-likeness and

92   prior knowledge of potential protein-protein disruptors[7]. A threshold value was set to

93   select actives with CD80$\geq$30% and CD86$\geq$20% cut-off for the Normalized Percent

94   Inhibition**.** Based on this criterion, 33 actives belonging to nine scaffolds were

95   identified from the screen (**Fig.1e, f**). **Fig.1g** depicts flow diagram of step-wise

96   filtering process. After eliminating singleton scaffolds; we identified hits that belonged

97   primarily to three scaffolds namely amino pyrimidine (**AP**), phenoxy acetamide (**PA**)

98   and bi-aryl heteroaryl carbamate (**BC**), which comprised of 20 compounds (**Supp**

99   **Table 1**), and these were selected for resynthesis (**Sup. Fig. S2**). Compounds from

100   all three scaffolds showed half maximal Inhibitory Concentration (IC$_{50}$) in nanomolar

101   ranges (**Fig. 1h; Supp Table 1**). Two independent experimental dose response data

102   correlated very well with an R^2 value of 0.9 (**Sup. Fig. S3).**

103   In summary, the biochemical screen identified more interaction inhibitors of Nef-

104   CD80 than Nef-CD86, which correlates well the MST binding isotherms indicating

105   that the Nef-CD86 interaction is of higher affinity than the Nef-CD80 interaction. One

106   representative compound from each scaffold with high potency against Nef-CD80

107   interaction was chosen for further cell-based assays.

108

109   **Small molecules block Nef-mediated internalization of cell surface CD80/CD86**

110   **receptors**

111   Before starting efficacy studies, we evaluated the cytotoxicity of the compounds

112   (**AP5**, **PA4** and **BC5**), as measured by WST-1 (Water Soluble Tetrazolium-1) assay.

113   The cytotoxicity index at the highest concentration of 100 µM for 24 h was around

114   17% for **AP5** and **PA4** whereas **BC5** was around 20% (**Sup. Fig. S4**). The maximum

115   concentration tested was 100 µM, and the concentrations chosen for the efficacy

116   work were mostly non-toxic for the assay durations.

117   The cellular efficacy assay was developed based on observations from our previous

118   work: the delivery of cytoplasmic CD80/86 tail peptides into the cell cytoplasm was

119   able to compete with and abrogate Nef-mediated internalization of cell surface

120   CD80/86[25]. We expected the small molecules identified by the biochemical screen

121   to behave in similar fashion to the cytosolic peptides. Surface levels of CD80/86

122   receptors in cells in culture with or without Nef protein were determined, and we

4

123 observed a significant loss of surface levels of CD80 and CD86 in the presence of

124 Nef in at least 3 types of Antigen Presenting Cells (APCs), including monocytes (**Fig.**

125 **2a**), consistent with our previous work[25]. The loss of CD80/86 surface receptors was

126 not observed with delivery of other non-specific proteins such as ovalbumin and β-

127 lactoglobulin which confirms that the internalization of surface receptors CD80 and

128 CD86 was indeed due to Nef (**Sup. Fig. S5**). We used RAJI, a B-lymphocyte cell line

129 for our experiments since this cell line has high levels of CD80 and CD86, and chose

130 to focus on targeting on the Nef-CD80 interface.

131 To test the effect of the compounds on Nef-mediated CD80 down modulation, cells

132 were pre-treated with the **AP5**, **PA4** and **BC5** at two concentrations 10 and 100 µM

133 for 1 hour. Purified Nef protein was delivered into the cells and surface CD80 levels

134 were analyzed by flow cytometry. **AP5** inhibited Nef-mediated down modulation of

135 CD80 at both 10 µM (*$p \leq 0.05$) and 100 µM (**$p \leq 0.01$) thereby restoring CD80

136 levels. Compounds **PA4** and **BC5** also showed a significant restoration (*$p \leq 0.05$) of

137 surface CD80 levels only at 100 µM (**Fig. 2b**).

138 We further validated the ability of these three compounds to reverse the effects of

139 Nef in RAJI cells transduced with Nef-containing virus (YFP-tagged Nef) or Nef-

140 deficient control virus (expressing only YFP). RAJI cells were pre-treated with **AP5,**

141 **PA4** and **BC5** for 24 hours' prior-exposure to virus and further incubated with virus

142 for 96h and then surface levels of CD80 receptors were estimated by flow cytometry,

143 there was ~50% loss of CD80 surface receptors in cells transduced with Nef-

144 containing virus as compared to control Nef-deficient virus infected cells. In cells

145 pre-treated with compounds, all 3 compounds significantly reversed Nef-mediated

146 internalization of CD80 receptors at 100 µM (**Fig. 2c**).

147

Compound AP5 is a selective inhibitor for Nef-induced CD80 down modulation

148

149   Since Nef also downregulates other cell surface molecules such as MHC-I and

150   MHC-II in APCs and CD4 in T-cells, apart from CD80/86 during viral infection, we

151   determined the effect of these compounds on the levels of MHC-I[28] in Nef-

152   transduced APCs. After compound treatment, we observed that **PA4** and **BC5**

153   reversed Nef-mediated effect of MHC-I down modulation while **AP5** did not alter Nef-

154   mediated down regulation of MHC-I even at 100 µM concentration (**Fig. 2d**).

155   Together, these data suggested that while all compounds disrupted Nef interactions

156   with CD80 and prevented the down modulation of CD86, the Nef-activated cascade

157   that triggers MHC-I down modulation was reversed only by **PA4** and **BC5.** This

158   indicates a very specific role for **AP5,** and a more broad-spectrum role for **PA4** and

159   **BC5**.

160

Restoration of T-cell activation in virus infected APCs by inhibitors

161

162   The co-stimulatory receptors CD80/86 along with MHC-I are needed for T-cell

163   activation. Previously it was shown that HIV-1 Nef-CD80/86 interaction impairs naïve

164   T-cell activation in *in-vivo* and *in-vitro* mouse systems[24]. We therefore ascertained if

165   the small molecule inhibitors were able to reverse Nef-mediated T-cell inactivation. A

166   co-culture assay system was adapted from a previously reported cell-based assay

167   for testing CD80 inhibitors[29] (**Fig. 3a**). Briefly, a non-replicative retroviral vector with

168   Nef transgene (**Sup Fig. 6 shows a** comparison of the non-replicative retroviral

169   vector with infectious HIV-1) was transduced in APCs to reduce CD80/86 levels at

170   the surface . These APCs were then co-cultured with T-cells in the presence of anti-

171   CD3 antibody and functional T-Cell activation was assessed by measuring IL-2

6

172   levels; relevant controls included T-cells alone, T-cells and B-cells in the absence of

173   anti- CD3 antibody (**Fig. 3b**).

174   We tested two different modes of addition of compounds: in the first mode, we pre-

175   treated APCs with 1, 10 and 100 µM of compounds (**AP5**, **PA4** and **BC5**) for 24h

176   then exposed the cells to Nef-carrying viral particles and assayed for IL-2 release.

177   We observed a dose dependent response with all 3 compounds **AP5, PA4** and **BC5**

178   showing a 4-fold increase (**$p \leq 0.01$) in IL-2 release at 100 µM as compared to Nef

179   virus control. At lower concentrations, compounds **AP5** and **PA4** showed 2-fold

180   increase (*$p \leq 0.05$) at 10 µM. **PA4** did not show significant IL-2 release at 10 µM

181   (**Fig. 3c**), thus, indicating restoration of T-cell activation in a dose dependent

182   manner.

183   In the second mode, we added compounds at 1, 10 and 100 µM concentrations post

184   viral exposure for 96h. **AP5** showed significant increase in IL-2 levels (3-fold) at all

185   concentrations when compared to Nef virus control (**$p \leq 0.01$), while **PA4** showed

186   2-fold increase (*$p \leq 0.05$) in IL-2 levels at 10 µM concentration and no changes in IL-

187   2 levels were observed in **BC5**. Interestingly, there was a reduction in IL-2 release at

188   100 µM dose in comparison to 1 µM and 10 µM, perhaps due to the toxicity

189   associated with this dose alongside viral effects (**Fig. 3d**). Thus far, these data

190   shows that **AP5** is a potent molecule both *in vitro* biochemical assays and in

191   restoring T-cell activation in an assay designed to assess the role of co-stimulation

192   dependent T-cell activation mediated by CD80/86.

193

194   **Structural insights into Nef-CD80 interaction**

195   To further understand the nature of inhibition of Nef-CD80 interaction by small

196   molecules such as AP5, we chose to analyze the structure of Nef-CD80-interaction

197   pocket. This requires the characterization of the interaction surface between Nef-

198   CD80 and an analysis of the ligand binding pocket for CD80. Despite repeated

199   attempts we were unable to obtain crystals of full-length Nef that diffracted better

200   than 4 Å, wherein the structure could be fully resolved. In the absence of a high-

201   resolution X-ray structure of the full-length Nef, we created a computational model of

202   Nef using a multi-template modeling approach. The major structural information was

203   acquired from the NMR structure PDB ID: 2NEF, as this structure has information for

204   the highly flexible loop region of the core domain (55-66) which contains important

205   interacting residues[30], as well as from the crystal structure PDB ID: 3RBB which

206   contains structural information of C-terminal folded core (residues 79-206). After

207   modeling, the lowest energy state structure was obtained by energy minimization via

208   SYBYL (Version 7.1) (Tripos Associates Inc.) and validated using PROCHECK.

209   PROCHECK results for the model shows more than 95% of the residues are in

210   allowed regions (79.9% in the strictly allowed region and 17.2% in partially allowed

211   region of the Ramachandran plot) which is better than the template structure (62.3%

212   in the strictly allowed region and 34.2% in partially allowed region of the

213   Ramachandran plot).

214   The structure of full-length Nef can be divided into two parts: a flexible and

215   structurally diverse N-terminal region of about 70 residues followed by a well-

216   conserved and folded core domain of about 120 amino acids. The core domain is the

217   only part of the Nef protein which has a stable tertiary structure. It forms an α-β

218   domain in which a central anti-parallel β-sheet of four strands (β1- β4) is flanked by

219   two long anti-parallel α helices (α4 and α5) and two short α helices (α1 and α5).

220   Residues 60-71 and 149-180 form flexible solvent exposed loops[19] (**Fig 4a**).

221   An independent verification of some aspects of the model was obtained from the

222   predicted Small Angle X-ray Scattering (SAXS) envelope of soluble Nef protein.

223   SAXS-patterns of full-length Nef were obtained at three different concentrations 1, 3

224   and 5 mg/ml (**Sup. Fig. S7a**). The Guinier plots at low angles appeared linear and

225   confirmed good data quality with no indication of protein aggregation (**inset Sup.**

226   **Fig. S7a**). The derived R_g values and the calculated maximum particle dimension

227   (D_{max}) values were reported. The R_g values extracted from the $P(r)$ function are in

228   agreement with the R_g values extracted from the Guinier region (**Sup. Table 2**). The

229   estimated R_g, D_{max} and molecular mass of the full-length Nef suggest a

230   concentration dependent increase in the R_g, D_{max} and molecular mass values

231   observed with Nef addition. Visual inspection of the normalized Kratky plot reveals

232   significant deviation from a bell-shaped profile which depict an inherent structural

233   flexibility of Nef (**Sup. Fig. S7b**). The averaged solution shape calculated using the 1

234   mg/ml scattering data clearly indicated that Nef is monomeric in solution. This

235   solution model also revealed a two-domain architecture, a large domain that is well

236   overlaid with the available 3D structure of folded C-terminal core (PDB ID: 3RBB)

237   (**Sup. Fig. S7c**)[31, 32]. The small domain corresponds to the N-terminal region

238   (residues 1-78) that contain a long flexible loop (residues 24-68). While structural

239   details of N-terminal region are available from NMR studies of a peptide regions from

240   residues 2-26[33] and 2-57[30], information about the relative orientation with C-terminal

241   core domain is missing. The SAXS data envelope along with the computational

242   model (**Fig. 4b**) provides structural information about spatial arrangement of the C-

243   terminal folded core and the flexible N-terminal region of full-length Nef in solution,

244   consistent with the computational predictions.

245

Identification of crucial residues involved in Nef-CD80 interaction surface

We next utilized the computational prediction of full-length Nef structure and

molecular docking studies with the cytoplasmic tail of CD80, to identify key residues

at the interaction surface. The putative binding sites of cytoplasmic CD80 to full

length Nef were mapped onto the template model utilizing SiteMap program for

binding site prediction. In characterizing binding sites, SiteMap provided quantitative

and graphical information in terms of site score and druggability score with properties

such as hydrogen bond donor, acceptor, hydrophobic and hydrophilic regions in the

predicted site. Docking studies of cytoplasmic tail region of CD80 with full length Nef

revealed that CD80 may interact with the interface between the flexible N-terminal

and C-terminal core domain. Potential binding sites were predicted with a good site

and druggability score (>0.5; **Sup. Table 3**).

The sites of interacting regions of Nef with other cellular proteins have been

previously characterized. A polyproline motif (68-78aa) present on the core domain

of Nef binds to the SH3 domain of Src kinases with high (nM to μM) affinity[34]. Other

than the polyproline motif within the core domain, a number of residues on the core

domain are involved in multiple interactions, such as $FPD_{126-128}$ with human

thioesterase and W_{61} and L_{115} with CD4[19]. An acidic cluster ($EEEE_{65}$) close to the

core domain is required for interaction with PACS1 and controls MHC-I down-

regulation[35,36]. The unstructured regions of Nef also provide an extensive accessible

surface that could be used to connect to other molecules. Since there is no prior

information about the binding pattern of Nef with CD80 it was necessary to score

each pose based on energy calculations. From the top ranked docked poses, the

best complex with the lowest energy (-246.30 kcal/mol) was chosen as the model

complex for Nef and CD80 interaction. In this predicted pose, CD80 cytoplasmic

10

271 region (indicated in cyan) interacts with the Site-1 and 2 residues in the core domain

272 of Nef (indicated in blue) (**Fig. 4c**). Based on this pose, the interacting residues

273 were mapped (**left inset Fig. 4c**). The side chains of site-1 residues $W_{61,}$ E_{68}, K_{99}

274 and R_{111} are in favourable position to interact with the N-terminus of the CD80

275 cytoplasmic tail. It should be noted that the residues K_{99} and R_{111} potentially make

276 polar contact with CD80 backbone carbonyl oxygen of F_4 and side chain hydroxyl

277 group of Y_2, respectively. In addition, the C-terminus of the CD80 cytoplasmic tail

278 potentially interact with E_{160} and D_{180} residues. The side of E_{160} potentially makes salt

279 bridge interaction with R_{16} and R_{23} of CD80 (**right inset Fig. 4c,**). Based on our *in-*

280 *silico* predictions we chose four residues that include, 3 from Site-1 ($W_{61,}$ K_{99} and

281 R_{111}) and one from Site-2 (E_{160}) for further analysis.

282

283 **Functional validation of predicted residues mediating Nef-CD80 interaction**

284 Single site mutant of Nef such as Nef^{W61A}, Nef^{K99A}, Nef^{R111A} and Nef^{E160A} were

285 designed and purified (**Sup. Fig. 8a & b**). These mutants were tested for their affinity

286 for CD80 peptide in the ELISA assay (**Fig. 5a**). Two mutants Nef^{K99A} and Nef^{R111A}

287 showed a loss of affinity to the CD80 peptide, whereas, the Nef^{W61A} and Nef^{E160A}

288 exhibited an affinity comparable to full length Nef^{WT}. These mutants were also

289 assessed for their ability to affect CD80 surface levels after delivery into APCs.

290 Indeed, the two mutants Nef^{K99A} and Nef^{R111A} did not show any reduction in CD80

291 levels, while Nef^{W61A} showed slightly lesser reduction in CD80 receptors and Nef^{E160A}

292 behaved similar to Nef^{WT} (**Fig. 5b**). Consistent with a key role for the K_{99} and R_{111} in

293 Nef-CD80 interactions, when transduced into APCs, Nef^{K99A} and Nef^{R111A} mutants

294 did not affect IL-2 release (**Fig. 5c**) thereby showing that T-cell activation is not

295 compromised by these mutant Nef variants. Surprisingly, while Nef^{W61A} down

11

296   modulated CD80 significantly, it did not result in a loss of T-cell activation. Since T-

297   cell activation assay requires a minimum of 4-5 h we reasoned that the Nef^{W61A}

298   protein delivered into the APCs may be less stable than the other isoforms for the 5

299   h required for this assay. Indeed, western blot analysis of the protein at 2 h versus 5

300   h in cell lysates shows that the level of Nef^{W61A} protein was drastically decreased

301   after 5 h, while the levels of the other Nef protein variants remained substantial (**Sup**

302   **Fig. 8c**). The other Nef^{E160A} mutant exhibited similar reduction of IL-2 release as

303   Nef^{WT} consistent with its ability to bind CD80 peptides as well as down modulate

304   CD80 at the APC surface (**Fig. 5b-d**).

305   The two mutants Nef^{W61A} and Nef^{R111A} also did not down regulate MHC-I receptors

306   as much as Nef^{WT}; whereas Nef^{K99A} and Nef^{E160A} exhibited a similar reduction in

307   MHC-I levels as Nef^{WT}, as assessed by surface MHC-I antibody staining (**Fig. 5d**).

308   W_{61} residue (W_{57} in Subtype B) has been previously reported to be important in CD4

309   down regulation and R_{111} residue (R_{106} in subtype B) is located in the oligomerization

310   domain of Nef. Many residues of Nef have been identified that promote interaction

311   with MHC-I, including W_{57} and R_{106} in subtype-B, NL4-3 strain, but their mutation did

312   not hinder MHC-I down regulation[37]. However, W_{61} and R_{111} residues in subtype C,

313   appear potentially important for Nef interaction with MHC-I, indicating subtle

314   differences in the modulation of host proteins by different Nef variants. Nevertheless,

315   these functional studies provide strong support to the predicted binding mode of

316   CD80 peptide with Nef via residues K_{99} and R_{111} in Site 1 (**Fig. 4c**). Mutation in these

317   residues leads to loss of binding capacity, resulting in the inability to down-modulate

318   CD80 thereby restoring T-cell activation function of the transduced APCs.

319

320   **AP5 ligand binding sites in Nef full length**

12

321   Considering the predictive potential of the computational model of Nef-CD80

322   interaction surface, the most potent binding inhibitor molecule, **AP5** was docked with

323   Nef protein to capture its binding pattern and important residues involved in

324   interaction. **AP5** fits nicely into the hydrophobic cavity formed by the residues W_{61},

325    $V_{71,}$ L_{115} and W_{118}, which are part of the N-terminal loop region and the α4 helix of

326   core domain (**Fig. 6a and inset**). The aromatic residues W_{61} and W_{118} mainly have π

327   -π stacking interaction with aromatic ring B in **AP5**. In addition to hydrophobic

328   interactions, the side chain of S_{50} and backbone of E_{68} form hydrogen bond

329   interaction with amine group of the ligand. The side chain of K_{99} from α3 helix of core

330   domain, interacts with the CF_3 (triflouro methyl) group. Moreover, AP5 binding site

331   overlaps with Site-1 of Nef-CD80 binding pocket, and the docking results showed

332   that the Nef-CD80 and Nef-AP5 binding sites are overlapping with two important

333   common residues such as W_{61} and K_{99}.

334   Consistent with these predictions, at 10 µM **AP5** was neither able to inhibit the

335   interaction between CD80 peptide and Nef^{W61A} mutant nor further reduce the residual

336   interaction of Nef^{K99A} and Nef^{R111A} mutants *in vitro* (**Fig. 6b**). However, AP5 was able

337   to displace both Nef^{WT} and Nef^{E160A} from CD80 peptides adsorbed on the ELISA

338   plate. Thus, W_{61} is an important residue for **AP5** binding to Nef. Furthermore, in

339   agreement with the predictions, **AP5** treatment did not result in any change in

340   surface levels of CD80 in APCs transduced with Nef^{W61A}, Nef^{K99A} and Nef^{R111A}

341   mutant proteins (**Fig. 6c**). The levels of IL-2 release in all three mutants Nef^{W61A},

342   Nef^{K99A} and Nef^{R111A} also remained unchanged, with the Nef^{W61A} mutant mimicking

343   the inhibition observed with wild type Nef. **AP5** restored IL-2 release in Nef^{E160A}

344   treated cells, comparable to Nef^{WT} (**Fig. 6d**), consistent with the inability of Nef^{E160A}

345   to affect neither CD80 nor **AP5** binding, thereby serving as a negative control. These

346 results predict and functionally validate the residues in the Nef protein that are

347 important for AP5 binding.

348

349 **Hit refinement of AP series**

350 We chose **AP5** as our starting point, given its nanomolar and micromolar potencies

351 in biochemical and cell-based assays respectively as well as specificity to CD80. An

352 initial hit refinement of **AP5** was conducted to understand the preliminary structure-

353 activity relationships (SAR). New analogs were synthesized in two series by

354 modifying the rings B and C with un/substituted aryl (heteroaryl) moieties, and

355 without -CF_3 group at the 6th position (**Fig. 7a**). In series-1, four analogs AP(S1-S4)

356 were prepared (**Sup. Fig. S2; Scheme-3**), where phenyl group (ring B) was placed

357 at the 4th position of ring A and varying the substitution pattern at 5th position (ring B).

358 In series-2, six analogs AP(S5-S10) were prepared by modifying both 4th and 5th

359 positions (**Sup. Fig. S2**; **Scheme-4**). Apart from these, another analog **AP-S11**

360 (**Sup. Fig. S2**; **Scheme-2**) was also synthesized where -CF_3 was maintained at the

361 6th position and substituted aryl rings at 4th and 5th positions.

362 All the synthesized molecules were evaluated for their effect on Nef-CD80/CD86

363 inhibition by ELISA. The analogs **AP(S1-S10)** without -CF_3 group at 6th position of

364 ring A didn't show any activity (**Fig. 7b**), however, the analog **AP-S11** with CF_3 at 6th

365 position of ring A showed the activity. These results disclosed that presence of CF_3

366 group at 6th position of ring A important for the activity (**Fig. 7c**). Moreover, docking

367 studies revealed that CF_3-group showed hydrophobic interactions with non-polar

368 residues such as W_{61}, L_{91}, I_{114} and L_{115} while *in vitro* and *in vivo* experiments

369 described above, suggested that these interactions are important for at least for the

370 inhibition of the down modulation capacity of Nef. These studies underline the

14

371   importance of the -CF$_3$ group at 6th position of ring A (**Fig.7a-c**). In conclusion, lead

372   compounds with potency in nanomolar range across the cell-based assay along with

373   acceptable solubility, permeability and pharmacokinetics parameters necessary for

374   further drug development and chemical perturbation of the Nef-CD80 interface, have

375   been developed.

376

377   **Discussion**

378   HIV-Nef plays an important role in the pathogenesis of HIV infections and

379   understanding its many functions in modifying the host cell surface has served as a

380   focal point of HIV research[38,39]. In earlier work we had determined that the presence

381   of wild type Nef in virus infected cells, promotes the loss of the co-stimulatory

382   proteins CD80/86 from the infected APC surface resulting in a loss of naïve T-cell

383   activation[23, 24, 25, 40]. Here we have identified potent small molecules that disrupt the

384   interaction of Nef with CD80 co-stimulatory receptors, and restore T-Cell activation

385   potential of virus-infected APCs. The three lead structures identified: **AP5**, **BC5** and

386   **PA4** belonged to three diverse scaffolds. While **PA4** and **BC5** are able to inhibit

387   both Nef mediated CD80 as well as MHC1 down-regulation, possibly indicating

388   different interaction points in Nef or counteracting Nef at more than one protein-

389   protein interface. **PA4** and **BC5** molecules are leads to explore for molecular

390   interaction promiscuity and investigating some of the multiple interactions of Nef.

391   Since **AP5** selectively inhibits Nef-mediated CD80 down-regulation, we chose to

392   pursue its detailed characterization in this study,

393

394   To gain an insight into the interactions of Nef with CD80, computational approaches

395   followed by experimental validation were used to identify possible binding sites on

396 Nef for both CD80 peptide and the small molecule inhibitor **AP5**. Due to the lack of

397 crystals with suitable diffraction properties to provide high-resolution structures, and

398 limited experimental information on full length Nef structure, possibly due to its

399 inherent flexibility we adopted a computational strategy. Full length Nef was modeled

400 by a multi-template computational approach, and their spatial conformation was

401 validated using the constraints obtained from SAXS experiments. The interaction site

402 for CD80 was obtained by docking of CD80 cytoplasmic tail with full length Nef

403 model, and a number of possible binding sites for its already known protein-protein

404 interaction sites were identified. These predictions provide key insights that could be

405 correlated with the experimental results, identifying key residues that are involved in

406 Nef-CD80 interaction. A caveat to be noted is that there is a limitation in finding the

407 best biologically relevant orientation of CD80 since the docking was restricted to only

408 the cytoplasmic tail peptide of CD80 which does not impose spatial conformation of

409 the full length CD80 embedded in the membrane. The free cytoplasmic CD80 region

410 fits in the energetically favorable orientation, given its steric constraints, providing

411 verifiable insights from mutation studies. In parallel the **AP5** docking results confirms

412 that W_{61} and K_{99} residues of Nef contributes to the interaction interface with this lead

413 molecule. Based on the Nef-CD80 and Nef-**AP5** docking results, hotspot residues

414 such as W_{61}, K_{99} and R_{111} were mutated. This revealed that the K_{99} and R_{111}

415 residues are crucial for CD80 binding and additionally, W_{61} plays an important role in

416 **AP5** binding. Since the binding sites for CD80 and **AP5** are overlapping, our study

417 provides a plausible view of the inhibitory mechanism, where AP5 interactions with

418 Nef would prevent its ability to associate with CD80, since they compete for the

419 same site. Ongoing efforts are aimed at improving the inhibitors with -CF_3 group in

420 **AP5** series and further validating these hits in *in vivo* studies.

16

421

422   Our results also indicate that Nef interaction with the co-stimulatory receptors

423   CD80/86 cytoplasmic tails are distinct from reported Nef –MHC-I interactions. Nef

424   interacts with MHC-I cytoplasmic via E_{62-65} and P_{78} residues[41], although subtype C

425   as shown here may utilize W_{61} and R_{111}. While Nef-MHC-1 interactions are

426   important, Chaudhry *et al*[24] showed that the kinetics of Nef down-modulation of MHC

427   molecules is slow as compared to the loss of co-stimulatory CD80/86 function. We

428   have shown that the interaction of Nef with the co-stimulatory CD80/86 is likely to be

429   critical for inhibiting the priming of the immune system towards naïve infections, and

430   hence may be critical for immune evasion strategy of the virus[42,43]. The chemical

431   tools developed here will allow such an interrogation in suitable animal models.

432

433   Once developed into drug-like chemicals, the leads we have identified from this

434   study would have significant impact in at least two scenarios where macrophages

435   play an important role for HIV-1 pathogenesis. One important application is in

436   maternal–fetal transmission and other in cases of early infection or persistent

437   infection resulting from viral mutations. 90% of HIV infection in children is through

438   Macrophage-tropic Maternal-fetal Transmission[44]. Nef plays a major role in vertical

439   transmission of Macrophage-tropic HIV-1 in mother to child, where the motifs for

440   receptor modulation were conserved in mother-to-infant *NEF* sequences. The

441   second scenario is in early stages of infection when viral load is low, the role of Nef-

442   mediated CD80 and CD86 down modulation from the antigen-presenting cell surface

443   could delay the onset of T-cell responses to provide the virus with a time window

444   sufficient for expansion. There is evidence that T-cells need co-stimulatory

445   molecules for optimal killing of target cells, thus even in cases of established

446   infection the removal of CD80 and CD86 from infected cell surfaces could reduce the

447   efficiency of T-cell responses[45]. If this is the case, blockade of this function by small-

448   molecule inhibitors of Nef-CD80/CD86-cytosolic tail interactions, could enhance

449   effectors antiviral immunity and delay the onset of disease in both pathophysiological

450   contexts.

451

452   Altogether, targeting this protein-protein interaction interface represents a promising

453   new therapeutic approach to bring forth a first in class set of inhibitors to foreshorten

454   the infection burden in HIV-1. The information gained from this integrated approach

455   of both computational and experimental study have set the foundation for further

456   ongoing efforts in synthesizing the next series of more drug-like inhibitors. We have

457   demonstrated a promising chemical starting point for building chemical tools and

458   drugs that can interfere with immunomodulatory consequences of HIV-1.

459

460   **Significance**

461   Our study aims to develop small molecule inhibitors that disrupt the interaction

462   interface between HIV-1 viral protein Nef and host CD80 / CD86 in Antigen

463   Presenting Cells (APC). The disruption of this interaction will makes infected APCs

464   more visible to the immune system, increasing cytotoxic lymphocyte activity on these

465   HIV-infected cells, potentially leading to viral clearance from macrophage reservoirs.

466   Here we identify and structurally characterize small molecule inhibitors that indeed

467   disrupt the protein-protein interaction interface of Nef-CD80 and restore the T-cell

468   activation capacity of infected APCs. These chemical tools serve as excellent

469   starting points that may be used to interrogate the role of Nef in HIV immune evasion

470   and contribute to first-in-class drugs for mitigating this resurgent disease

Author contributions

SM, ASK, TS, PPS and RAV contributed to project initiation and funding. SM and ASK contributed to the study design of biochemical screen and cell-based assays. PPS and RAV contributed to the medicinal chemistry study design. ARV contributed to the structural biology study design and supported this work at the CCBT. AUS, APN and AM contributed to compound screening and cell-based experimental work. SS, SA, GM, KRY and PPS contributed to chemical synthesis and structure activity relationship analyses. GA and RS contributed to the molecular modeling and docking studies. SR contributed to mutant study. NK performed the SAXS studies. SM, AUS and ASK wrote the manuscript, which was reviewed by RAV and ARV. Figures were prepared by AUS, SS, PPS, GA and NK.

Declaration of Interests

The authors declare No competing interest.

496
497

498   **Figure Legends**

499
500   **Fig. 1 Nef directly interacts with the cytoplasmic tail peptides of CD80/86.**

501   **a)**   Illustration shows the CD80 and CD86 receptors with their extracellular,

502   transmembrane and cytosolic tail region marked. The 20-mer peptide region of CD80

503   (PRCRERRRNERLRRESVRPV, 269 to 288 a.a) and CD86

504   (LWKWKKKKRPRNSYKCGTNT, 267-286 a.a) is highlighted within the cytoplasmic

505   tail domain (**b**) Graph shows direct binding of Nef to CD80 as measured by

506   Microscale scale thermophoresis (MST). CD80 peptide was titrated from 950 µM in

507   2-fold dilutions upto 16 points against a fixed Nef concentration (35 nM) in the final

508   reaction volume. A curve with upper saturation with kD=27 µM was obtained; x axis=

509   peptide concentration (nM) and y axis= percentage normalized fluorescence

510   (ΔFnorm); Plots represent the mean ± SD (error bars) from three independent

511   experiments **(c)** Similarly, CD86 peptide was titrated from 10 µM with a 2-fold serial

512   dilution upto 16 points against a fixed Nef concentration (35 nM). A sigmoidal curve

513   with kD=112 nM, showing higher affinity as compared to CD80. **(d)** Graph shows

514   ELISA assay where change in OD is observed when the immobilized CD80 and

515   CD86 cytosolic peptides binds to Nef. The OD measurement was done at 450nm.

516   CD74, a negative peptide control shows minimal OD value **(e)** Graph shows

517   Normalized Percentage Index (NPI) on a normal distribution curve for statistical

518   significance of active compounds across qualified plates showing CD80 actives. X

519   axis= the number of compounds screened in ELISA assay; y axis= normalized

520   percentage Inhibition of compounds; of Z-factor>0.5 analysis was used to qualify the

521   plates. Compounds with NPI>30% for CD80 was considered as hits **(f)** Similarly,

522   NPI normal distribution curve for CD86 with Cutoff percentage for CD86 NPI>20%

523   was considered as hits **(g)** Scheme shows the hits belonging to 9 scaffolds that

524   were identified in the primary screen **(h)** Dose response curve of a hit compound

525   from "AP" scaffold; x axis= log concentration of compounds; y axis= Normalized

526   percentage Inhibition, (inset) Structure of AP5 compound and its molecular

527   properties

528   **Fig. 2: Cell based assay screening of active compounds from ELISA**.

529   **(a)** Nef mediated down-regulation of surface CD80 or CD86 in 3 different cell lines as

530   indicated. FACS data showing the normalized surface levels of CD80; I_x/I (y axis)

531   where I_x is the average fluorescence intensity in the indicated condition (from a

532   triplicate) and I is the Median of normalized negative control (No Nef control) **(b)**

533   FACS data shows restoration of CD80 receptors in RAJI cell line after pre-treatment

534   with 3 representative compounds **AP5, PA4 and BC5** at 10 and 100 µM for 24 h and

535   analysis after 2 h post Nef protein delivery **(c)** RAJI cell line was infected with viral

536   particles (Nef-YFP and YFP alone control cells) in viral infection assay and surface

537   CD80 receptors with compounds were measured by flow cytometry **(d)** Effects of

538   inhibitors on Nef-MHC-I interactions. RAJI cells were treated with compounds at 100

539   µM and then stained with anti-MHC-I antibody. MHC-I was detected by flow

540   cytometry and shown as I_x/I plots. Compound **AP5** shows no restoration of MHC-I

541   indicating its specificity for the Nef-CD80 interface.

542   **Fig. 3: Restoration of functional T-cell activation in a viral infection assay**

543   **(a)** Schematic of a functional assay for screening of compounds that disrupt Nef-

544   CD80/86 interactions in a virally-infected cell. Functional T-Cell activation is based

545   on APC-T cell co-cultures. The APC has CD80/86 and concurrent presence of anti-

546   CD3 antibody promotes T-cell activation (as measured via IL-2) in co-cultured T-cells

21

547 **(b)** Graph shows cytokine release in functional T-cell activation assay where antigen

548 presenting cell RAJI (B-cells) and Jurkat-cells (T cells) were co-cultured as indicated

549 (with/without anti-CD3 antibody); T-cells alone, B-cells alone controls do not show

550 measurable IL-2 release. **(c)** Graph shows quantification of cytokine (IL-2) released

551 after T-cells and B-cells co-culture for 3 h; here B-cells were pretreated with the

552 indicated concentrations (1, 10, 100 µM) of compounds for 24 h followed by viral

553 infection for 96 h **(d)** Graph shows quantification of cytokine (IL-2) released after T-

554 cells and B-cells co-culture for 3 h; here B-cells were first infected with virus for 96h

555 and then treated with compounds at 1, 10, 100 µM for 24 h. IL-2 release (pg/ml) was

556 determined by ELISA by plotting against an IL-2 standard curve. Note: viral infection

557 reduces IL-2 release, and all 3 compounds showed a dose dependent restoration of

558 IL-2 release. **AP5** showed IL-2 release at 1 µM.

559 **Fig. 4: Modelling of Nef with multi-template computational approach**

560 **(a)** Cartoon representation of the predicted structure of Nef shows flexible N-terminal

561 region and well-conserved core domain, colored in accordance with their position (N-

562 terminal in blue to C-terminal in red) with respective α-helices and β-sheets as

563 indicated. **(b)** The *ab initio* shape of the solution structure of the Nef (blue color) from

564 the SAXS data (grey surface) fits well with the computational model (cartoon

565 representation) **(c)** Surface representation of HIV-1 Nef is depicted with the best

566 CD80 binding pose. CD80 peptide in a docked pose (cyan color) in Nef obtained

567 using SiteMap program. The inset shows the important residues of Nef involved in

568 interaction with CD80 at Sites 1 and 2.

569 **Fig. 5: Evaluation of interaction between CD80 and Nef mutants in biochemical**

570 **and cell-based assays**

571 **(a)** Graph shows colorimetric signal of immobilized CD80 cytosolic peptide upon

22

572 binding to Nef^{WT} or Nef mutants as measured by ELISA at OD450nm. Two mutants

573 Nef^{K99A} and Nef^{R111A} showed reduced affinity to CD80 peptide **(b)** Graph shows

574 FACS data of surface levels of CD80 receptors in RAJI cell line after delivery of

575 Nef^{WT} or Nef mutant protein delivery. No significant down regulation seen with

576 mutants Nef^{K99A} and Nef^{R111A} **(c)** Graph shows the levels cytokine (IL-2) released in

577 supernatants of cells in the co-culture functional T-cell activation assay after delivery

578 of the Nef mutants as compared to the wild type Nef protein. **(d)** Graph shows FACS

579 data of MHC-1 levels after delivery with Nef^{WT}and mutants. Nef^{WT} or mutants were

580 delivered into RAJI cells using Chariot^{TM} delivery reagent. MHC-I was detected by

581 flow cytometry and shown as Ix/I plots.

582 **Fig. 6: Structural and functional evaluation of the interaction between Nef and**

583 **AP5**

584 **(a)** Structural and functional evaluation of the interaction between Nef and AP5The

585 Surface representation of HIV-1 Nef depicting **AP5** ligand (green color) binding. The

586 binding site of **AP5** molecule overlaps with the CD80 binding site (Site-1). The inset

587 shows the important residues for the interaction between AP5 and Nef. The non-

588 polar residues such as $W_{61,}$ $L_{91,}$ I_{109} and L_{115} contribute to hydrophobic interactions

589 with CF_3. **AP5** ligand docking studies shows that the binding interactions occurs

590 between the α4 and α5 helices along with few residues such as W_{61}, E_{65} and R_{111}

591 which are crucial for **AP5**-Nef interaction **(b)** Graph shows colorimetric signal of

592 immobilized CD80 cytosolic peptide upon binding to Nef^{WT} or Nef mutants in the

593 presence /absence of 10 μM AP5 as measured by ELISA at OD450 nm. (g) Graph

594 shows surface levels of CD80 receptors in RAJI cell line after the delivery of Nef^{WT} or

595 Nef mutant protein delivery as measured by FACS in the presence /absence of 10

596 μM AP5. Nef^{W61A}, Nef^{K99A} and Nef^{R111} did not show any further change in CD80

23

597   levels with **AP5** addition. **(c)** Graph shows cytokine (IL-2) release in supernatants

598   after the co-culture T-cell activation assay. RAJI cells were pre-treated with 10 μM

599   AP5 for 1 h and then the cells were delivered with Nef mutants or wild type Nef

600   protein for 2 h before co-culture with Jurkat T-cells for 3 h. The IL-2 levels remain

601   unchanged with and without addition of **AP5** compound in all three mutants Nef^{W61A},

602   Nef^{K99A} and Nef^{R111}. Reduction in IL-2 seen with mutant Nef^{E160A} comparable to

603   Nef^{WT}.

604   **Fig. 7**: **SAR and Hit refinement with AP5 as a template (a)** Scheme shows

605   Medicinal chemistry approach for hit refinement of **AP5** showing two series of

606   compounds **(b)** Summary of SAR strategy to design compounds similar to **AP5**

607   **structure** with modifications made on rings A, B and C as indicated. The

608   synthesized molecules were evaluated for their effect on Nef-CD80/CD86 inhibition

609   **(c)** Heat map table showing SAR with synthesized compounds. The various

610   substitutions in rings A, B and C are indicated as well as their activity in the ELISA

611   and cell-based assays

612

24

613 **STAR methods**

614

615 **Materials and Reagents:**

616 96-well maxisorp ELISA plates (NUNC, cat#449824,), small molecule inhibitors

617 (synthesized by IIIM, Jammu), DMSO (Sigma, cat#D2650), Anti-Nef Antibody (from

618 ICGEB), DAR-HRP (Jackson Immunoresearch, cat#711-035-152), Tecan ELISA

619 reader. The following commercially synthesized peptides (Peptron Inc., South Korea)

620 were used: CD80 cytosolic tail peptide: PRCRERRRNERLRRESVRPV (20-mer),

621 CD86 cytosolic tail peptide: LWKWKKKKRPRNSYKCGTNT (20-mer), CD74, a non-

622 specific peptide: MHRRRSRSCREDQKPVMDDQRDLISNNEQL (30-mer). Nef

623 construct was cloned at ICGEB, rF2-Nef protein (HIV-1 Subtype C) cloned into

624 pET28 vector (Novagen, cat#69865) at NcoI and XhoI sites with 6XHis tag at C-

625 terminal end. Nef and all Nef variant proteins were expressed in E. coli Rosetta

626 strain containing pRARE that codes for t-RNAs corresponding to rare Arginine

627 codons in the bacterium. The growth and/or expression medium used were Luria

628 Broth. The antibiotics used were kanamycin (50µg/ml) for Nef plasmid selection and

629 chloramphenicol (25µg/ul) for pRARE selection, IPTG induction, Akta FPLC –Affinity

630 and Size exclusion chromatography for protein purification.

631 **Cell lines**- RAJI B lymphocytic, Burkitt's lymphoma cell line (NIH AIDS reagent

632 cat#ARP-9944), Jurkat T cells (ATCC, cat#TIB-152), for cell-based assays,

633 HEK293T (ATCC CRL-3216) was used for transfection of viral clones and production

634 of viral particles.

635 *Cell culture reagents*- RPMI 1640, FBS, glutamine, Penstrep (from Gibco),

636 Chariot™ delivery reagent (active motif, cat#30100) was used for protein delivery

637 into cells. Viafect (Promega, cat#E4982) reagent was used for DNA transfection,

638 lentiX concentrator (clontech, cat#631231), lentiblast reagent (OZ

25

639 biosciences,cat#LB00500), DMEM (Gibco), WST-1 reagent (Roche), anti-CD80 and

640 anti-CD86-biotinylated antibody (Ebioscience, cat# 13-0809-82 and 13-0869-82),

641 SAV-APC (Ebioscience, cat#17-4317-82), anti-CD3 antibody (Biolegend, 317302),

642 western blot materials (Biorad), Chemiluminescent reagent (Pierce, cat#32109), GE

643 Image Quant, human IL-2 ELISA kit (Biolegend, cat#431808), Plasmid prep kit

644 (Qiagen), biotinylated anti-human MHC-I (HLA-A, B, C) antibody (biolegend,

645 cat#311402).

646 **Chemical Compound Synthesis**

647 The 25 active hits belong to three scaffolds namely amino pyrimidine (**AP**), biaryl

648 (heteroaryl) carbamate (**BC**) and phenoxy acetamide (**PA**) has been selected and

649 details regarding the strategies applied for the synthesis of hits and hit optimized

650 compounds has been provided in Scheme 1-8 (Supplementary data).

651 The synthesis started with amino pyrimidine (AP) scaffolds, where five hits were

652 synthesized and their synthetic strategy has been given in Scheme 1 and 2. The

653 synthesis started with commercially available 2-chloro-5-bromopyrimidine **1** as the

654 starting material which was treated with ethanethiol **2** afforded intermediate **3**

655 (Scheme 1). The intermediate **3** was then subjected to Suzuki coupling with aryl

656 boronic acid **4** provided 5-aryl pyrimidine **5**. The compound **5** was then oxidized with

657 *m*-CPBA to corresponding sulfoxide **6** followed by nucleophilic substitution afforded

658 key intermediate **7**, which on reaction with acetylacetone provided **AP1**. In the next

659 attempt, the intermediate **7** on reaction with substituted aldehydes provided **AP2** and

660 **AP3**. In another attempt, the 2-chloro-5-bromopyrimidine **1** was converted into **AP4**

661 in two steps i) nucleophilic substitution with dimethyl amine; ii) Suzuki coupling with

662 phenyl boronic acid. The synthesis of **AP5** required the quite different strategy and is

663 shown in Scheme 2. The synthesis started with commercially available resorcinol **11**

26

664   which was undergoes acetylation followed by reduction gave intermediate **13**. The

665   intermediate **13** was treated with 4-methoxyphenyl acetonitrile **14** to get acylated

666   intermediate **15** which on treatment with trifluoroacetic anhydride underwent

667   cyclization to generate the chromone based key intermediate **16** followed by the

668   methylation of hydroxyl group to get **17**, which on reaction with guanidine

669   hydrochloride to afford the hit **AP5**.

670   For the initial hit refinement, we started synthesis with commercially available

671   2-aminopyrimidine **28** which on reaction with phenyl boronic acid **4b** with

672   methodology was developed in the presence of light and $K_2S_2O_8$ gave intermediate

673   **29**. Intermediate **29** was brominated in the presence of *N*-bromosuccinamide (NBS)

674   provided the intermediate **30**. The final targeted compounds **AP(S1-S4)** were

675   synthesized in good to moderate yields from the reaction of compound **30** with

676   substituted phenyl and heterocyclic boronic acids **4** under Suzuki conditions to

677   provide final compounds **AP (S1-S4,** scheme-3). For series-2, sequence of synthesis

678   began with 2-amino-4-chloropyrimidine **31** which underwent Suzuki coupling reaction

679   with un/substituted aryl and heteroaryl boronic acids **4** to get intermediate **32** which

680   on reaction with NBS provided intermediate **33**. The brominated intermediate **33** was

681   subjected to Suzuki couplings with a range of aryl and heteroaryl boronic acids **4** to

682   provide final compounds **AP (S5-S10,** Scheme-4).

683   In the case of biaryl (heteroaryl) carbamate (BC), seven hits were synthesized

684   (Schemes 5-6). The synthesis started with commercially available

685   phenylchloroformate **18** which on treatment with benzo[d]oxazole-2(3H)-thione **19** in

686   the presence of base to give the hit **BC1** (Scheme 5). All other hit molecules from

687   **BC3** to **BC7** and **BC10** were synthesized in the similar fashion, different substituted

688   chloroformates **18** reacted with substituted anilines **20** to afford the targeted hits

689   (Scheme 6).

690   In case of phenoxyacetamide (PA), syntheses of eight hits were accomplished as

691   outlined in Scheme 7 and 8. Hit molecules like **PA2**, **3**, **5**, **6** and **7 (Scheme 7)** were

692   synthesized in two steps. i) by treating substituted anilines **20** with different

693   chloroacetyl chloride in the presence of base at room temperature followed by; ii)

694   coupling with substituted phenols **23**. For the synthesis of hits **PA1, 8 and 10,** the

695   synthesized involves four steps. The substituted phenols **23** coupled with substituted

696   2-chloroethylacetate **24** to form intermediate **25**, which on hydrolysis gave

697   intermediate **26**. The intermediate **26** was converted into corresponding aryl chloride

698   **27** and then coupled with substituted anilines **20** to get the desired hits **PA1, 8** and

699   **10** (Scheme 8).

700   The identified hits such as **BC2, 6 and 8**, and **PA4** and **PA9** were not synthesized

701   and were procured in somewhat large quantities from the original commercial

702   vendors because of the unavailability of the starting materials. These hits were

703   characterized by using NMR and Mass spectroscopy and then were taken up for

704   validation study.

705   ***Compound stock and storage-*** All compounds were dissolved 100% DMSO to

706   make a 10mM stock. Multiple aliquots were prepared from mother stock to avoid

707   multiple freeze-thaw cycles and were stored at -80°C

708   **Expression and Purification of recombinant Nef**

709   HIV-1 Nef gene sequence was cloned into pET28b expression vector with antibiotic

710   resistance to chloramphenicol (25µg/ml) and kanamycin (50µg/ml) and recombinant

711   Nef-His tag protein was expressed in *E. coli* Rosetta strain [OD600~0.5-0.6]. IPTG

712   induction (0.2mM) was done for 4h at 28ºC. The cells were spun down at 10000rpm

28

713   for 15minand pellet stored at -80ºC. The protein was purified in 20mM Tris HCl,

714   150mM, NaCl, 3 mM DTT, 5% glycerol, 0.2% Tween-20 in a Ni-NTA column and gel

715   filtration chromatography on Sepharose-75pg (GE) in Akta FPLC purifier. Nef protein

716   with single mutants W61A, K99A, R111 and E160A were designed by site-directed

717   mutagenesis. The buffer conditions were same as full length WT-Nef.

Mutant	Primers used
W57A	F: GAT TGT GCT GCG CCG GAA GCG C
	R: GCG CTT CCG GCG CAG CAC AAT C
K94A	F: AAA GAA GCG GGG GGA CTG GAA GGG
	R: CCC TTC CAG TCC CCC CGC TTC TTT
R106A	F: CTAAGAAAGCGCAAGAGATCCTTGATTTG
	R: CAAATCAAGGATCTCTTGCGCTTTCTTAG
E155A	F: GCA GTA GAA GCG GCC AAC GAA GGA G
	R: CTC CTT CGT TGG CCG CTT CTA CTG C

718

Microscale Thermophoresis (MST)

719

720   Full length Nef was labeled with lysine NT-647-NHS fluorescent dye using the

721   Monolith NT.115 Protein Labeling Kit (NanoTemper Technologies). A Capillary

722   Scanning was performed to check the optimal fluorescence intensity of the labelled

723   protein for titration with the ligand. For the direct binding assay, a final concentration

724   of labelled 35nM Nef protein was titrated against a 16-point 2-fold serial dilution

725   series starting from 950 μM for CD80 peptide and for CD86 a final concentration of

726   labelled 25nM Nef protein was titrated against a 16-point 2-fold serial dilution series

727   starting from 10 μM. The compound was titrated against the protein-peptide at16-

728   point dilution. All samples were prepared by centrifuging at 10000 rpm for 5 min at

729   4˚C and 10 μl of the supernatant was loaded into premium glass capillaries

730   (NanoTemper Technologies). MST runs were performed at MST power of 60% and

731   excitation power of 50%, using a Monolith NT.115 NanoTemper Technologies. The

732   data was analyzed using NanoTemper analysis softwareMO. Affinity Analysis v2.2.4.

733   Kd values were determined using T-jump and thermophoresis settings. The change

734   in thermophoresis between each sample dilution was represented as normalized

735   fluorescence (ΔF_{norm}), which is defined as F_{hot}/F_{cold}, where F_{cold} is the control and

736   F_{hot} is the experimental condition. The binding kinetics to non-fluorescent ligand

737   causes a change in thermophoresis which is determined by area in the curve under

738   steady-state conditions to yield a binding curve.

739   **Primary screening by Indirect Enzyme-linked immunosorbent assay (ELISA)**

740   An indirect ELISA was performed to measure the interaction of Nef-CD80/CD86 and

741   their disruption with addition of compounds.CD80, CD86 and a non-specific control

742   peptide derived from the cytoplasmic tail of CD74 peptides were separately

743   immobilized at 10 µM concentration onto 96-well micro-titer plate and incubated

744   overnight at 4°C. 5% blotto was used as blocking buffer to reduce the background

745   interference. Blotto was completely removed with PBS-Tween (0.1%) washes. 10

746   µM of Nef protein and 10 µM of compounds were pre-incubated at RT for 1hour and

747   added onto peptide coated wells for 1hour incubation. Compounds were diluted in

748   2.5% blotto and were screened at a concentration of 10µM. After each addition step

749   PBS-T washes were done. DMSO in 2.5% blotto as vehicle control and plate

750   background (no coating) were used as negative control. In subsequent steps the

751   plates were incubated with primary anti-Nef antibody and secondary antibody with

752   HRP. The TMB substrate was added which reacts with HRP to produce a coloured

753   product within 15minutes. The reaction was stopped with 1N sulphuric acid and the

754   absorbance at 450nm was recorded with Tecan infinite 200 PRO plate reader.

755   MATLAB 7.5 program was used to pick the active compounds. The program

756   assessed the robustness of the screened plate using Z-factor (for qualifying plate)

757   and Z score for active compounds, and Normalized percent inhibition to determine

758   the compound activity.

759   *Robustness of screen*

760   The plate controls showing a Z factor >0.5 was considered to qualify for further

761   analysis. The activity of compounds was determined with the Normalized Percent

762   Inhibition (NPI) and Z scores were used to assess the efficacy of the compounds in

763   the screen: Z-score: $(Ix - \mu D)/ \sigma D$

764   Normalized inhibition (NPI): $((Ix - \mu D)/ \mu D)*100$

765   Where, IX: Intensity of triplicate x (first, second or third) represented as either A/B/C

766   μD: Mean of negative control

767   σD: Standard deviation of triplicates of negative control

768   The compounds identified as 'hits' in primary screen were defined as those

769   displaying more than 30% and 20% inhibition for CD80 and CD86 respectively and

770   two of three repeats of a particular compound should have Z score between - 2 and -

771   8.

772   ***Determination of IC$_{50}$ for active compounds***- The active compounds from primary

773   screen were tested for dose response with 10-fold dilution for an 11-point curve from

774   10μM to nanomolar concentration. Compounds showing an IC$_{50}$ in nanomolar

775   concentrations were further tested in cell-based assay.

776   **WST assay for quantification of cell viability and toxicity**

777   50000 cells per well were seeded in a 96 well plate. 1%Triton X (control) and

778   compounds were treated at 100 μM in triplicates in 100 μl media and incubated for

779   the 24 hours' timepoint. 10 μl of WST-1 reagent per well was added and incubated

780   for 3hrs.Absorbance read at 450nm with reference 620nm. The media alone control

781   was used to normalize all the wells. The cells alone control was the high control and

782   triton treated cells were the low control or negative control.

783   The formula used to calculate the percentage toxicity:

784   (Average $_{(X)}$ – Average $_{(high\ control)}$ / Average $_{(low\ control)}$ – Average $_{(high\ control)}$)*100

785   Where, Average$_{(X)}$= average OD of individual test; Average $_{(high\ control)}$ = average OD

786   of cells alone control; Average $_{(low\ control)}$ = average OD of cells with 1% triton X

787   **Measurement of surface levels of CD80/CD86 receptor by flow cytometry**

788   Nef protein was delivered into RAJI B cells using Chariot^{TM} protein delivery reagent

789   according to manufacturer's protocol (Active Motif). In brief, $1.5X10^5$ cells were

790   layered with protein-delivery reagent complex, incubated and complete media

791   (RPMI+10% FBS) was added. The cells were then harvested and stained with CD80

792   or CD86 biotinylated antibody or isotype control followed by Streptavidin-APC at 4°C

793   and flow profile acquisition was done on Gallios Flow Cytometer (Beckman Coulter).

794   Data was analyzed by FlowJo LLC software. Surface levels of CD80 and CD86 was

795   calculated by normalizing raw fluorescent measurements relative to controls

796   (Normalized Inhibition of Down-regulation). To test compounds, two concentrations

797   10 and 100μM were pre-treated on cells for 1 hour and then 50 μg of Nef was

798   delivered with method described and quantified by flow cytometry.

799   The potential actives from the plates were selected based on the following metrics.

800   a) Z score:

$$Z\text{-score:} \qquad \frac{I_X - \mu_D}{\sigma_D}$$

801   Where I_x is the measurement of each triplicate, μD: mean of population and σD:

802   Standard deviation of population (excluding the positive and negative control). Z

803   score was used to select hits reversal of CD80/86 downregulation by Nef.

804   Compound repeats were qualified by Z score selection, with a Z score between 1.5

805   to -1.2. Each graph was calculated with student t-test using Graphpad prism 7.0 (*p

32

806 ≤0.05; **p ≤ 0.01; ***p ≤ 0.001) was used to determine the significant difference

807 between the means of control group and treatment groups.

808 ***Calculation of surface CD80 and CD86 down regulation*-** was calculated by

809 normalizing raw fluorescent measurements relative to controls (Normalized Inhibition

810 of Down-regulation)

811 $$NID= I_x/I$$

812 Where I_x, is the raw measurement each triplicate and I is the mean of the

813 measurements on the positive control.

814 **Virus particle generation**

815 *HEK293T transfection*: The 4 retroviral components present in the following

816 plasmids, pVSV-G (envelope), p-gag-pol (packaging), pMSCV-Nef-YFP (HIV-1 F2

817 isolate-based retroviral clones harboring nef sequence), pMSCV-YFP (control) were

818 transfected into individual recombinant bacteria and cultured in LB for plasmid

819 isolation (miniprep Qiagen). The plasmid concentration was checked by

820 NanoDrop™.

821 *Virus particle generation*: To generate recombinant retroviral particles, HEK293T

822 were seeded into 100mm dish with $5X10^6$ cells on day 1. At 80% confluency, Viafect

823 ™ transfection reagent with 15µg of DNA vectors consisting of p-gag pol, pVSV-G

824 and YFP or Nef-YFP in 3:1:4 ratios was layered over cells with DMEM (5% FBS).

825 The cells are incubated for 72h. The cells were observed under fluorescence

826 microscope for YFP expression to estimate the percentage transfection. The cell

827 supernatant was collected and concentrated with Lenti-X™ reagent (as per

828 manufacturer's protocol). The visible pellet was reconstituted with minimal volume of

829 PBS (1X) to make a concentrated viral stock. The stock was titrated in 3-fold serial

830 dilution onto HEK293T ($1X10^5$) cells/ well in a 24 well plate. Polybrene (8µg/ml) was

831 added to cells along with DMEM (5%FBS) media. After 72h, the cells were harvested

832 and analyzed on Gallios flow cytometer. The fluorescent population was gated and

833 analyzed against the cells alone. The infection percentage above 30% and below

834 0.5% is omitted. The higher titer tends to be underestimated; lower titer falls too

835 close to the background. The average of the titer was used to calculate the viral units

836 present in the stock using the low formula:

837

$$TU/ml = \frac{\left\{ \text{Number of target cells (count at day1)} \times \frac{\text{\% of YFP-positive cells}}{100} \right\}}{\text{Volume of supernatant in ml}}$$

838

839 **_Functional T-cell activation Assay_** - RAJI cells were infected with MOI-0.02 of viral

840 stock of control YFP virus or Nef-YFP containing virus and incubated in a 24-well cell

841 bind plate. Additionally, LentiBlast^{TM} reagent A and B was added in 1:1 ratio to the

842 cells and incubated for 48 to 96h. The cells showed YFP signal post infection. The

843 cells were harvested and stained for CD80 and CD86 and analyzed by flow

844 cytometry and the percentage down-modulation of the receptors was calculated with

845 median values.

846 Virus infected RAJI- cells was co-cultured with Jurkat T cells (1:1 ratio, 2.5×10^5 cells)

847 in the presence of 0.06 µg/mL of anti-CD3 antibody (OKT3 clone, BioLegend®) in

848 final volume of 200 µl and incubated for 3h for 37°C in a 96 well plate and the

849 supernatant was harvested by centrifuging twice at 4000 rpm. IL-2 Cytokine release

850 in the supernatant was quantified by BioLegend® kit-based ELISA method and ODs

851 were measured in Tecan infinite 200 PRO plate reader.

852 *Testing of compounds in viral assay for functional T-cell activation assay*- Pre-

853 treatment with compounds **AP5, PA4** and **BC5** at 1, 10 and 100 µM concentrations

854 was performed for 24h before Nef viral transduction in RAJI cells. Vehicle control

855 cells were pre-treated with 0.5% DMSO. Post-treatment of compounds for 24h was

856 done after 96h of viral infection.

857 **Staining of surface MHC-I antibody**

858 RAJI cells were pre-treated with compounds **AP5, PA4** and **BC5** at 100 µM and 50

859 µg Nef was delivered with Chariot^TM reagent. The cells were stained for receptors

860 with anti-human MHC-I biotinylated (HLA-A, B, C, clone W6/32) BioLegend®

861 antibody and secondary streptavidin APC and was run on Gallios flow cytometer and

862 the surface levels MHC-I was quantified. The percentage down regulation recovery

863 of MHC-I receptors was analyzed.

864 **Modelling of full-length Nef**

865 To build a full-length Nef protein, multi-template modelling approach was performed,

866 where more than one experimentally determined structure was utilized for building

867 the model. For the N-terminal part, NMR structure of Nef anchor domain(1QA5) and

868 for core domain, the NMR structure of HIV-1 Nef (2NEF: A) and X-ray structure HIV-

869 1 NEF protein, in complex with engineered HCK SH3 domain (3RBB: A) are used as

870 templates. Among the three templates, major structural information is acquired from

871 2NEF structure which covers maximum region of core domain. The tool

872 MODELLER7 (version 9v8) was used to obtain the full-length Nef model. After

873 modeling, the lowest energy state structure was further energy minimized through

874 SYBYL (Version 7.1) (Tripos Associates Inc.) and validated using PROCHECK[46]

875 **Deciphering the residues necessary for Nef - CD80 interaction by docking**

876 **studies**

877 The modeled full-length Nef protein is utilized for examining the potential-ligand

878 association site using the SiteMap[c] tool in Schrödinger software. SiteMap identifies

879 potential peptide/ligand binding sites considering van der Waals forces and hydrogen

880 donor∕acceptor characteristics. SiteScore is the most important property generated

881 by SiteMap, proven to be effective at identifying possible binding sites in 3D

882 structure. The prediction of the binding site is based on set of properties such as size

883 of the site, degrees of enclosure by the protein and exposure to solvent, tightness

884 with which the site points interact with the receptor, hydrophobic and hydrophilic

885 character of the site. The sitemap predictions are useful in identifying the possible

886 binding sites of CD80/CD86 cytoplasmic tails.

887 Further, docking studies were performed to identify the interactions of Nef protein

888 with co-stimulatory molecules CD80/CD86. This was achieved by modelling of

889 cytoplasmic regions of CD80/CD86 using I-TASSER server and protein-peptide

890 docking using BioLuminate module in Schrödinger software. Though numerous

891 information about the Nef interaction sites with other cell surface receptors are

892 available, the peptide is docked by blind docking approach where no guidance about

893 residues, that could potentially participate in interaction with CD80 was provided to

894 the program. The best docked pose is selected by energy minimization followed by

895 implicit solvent based energy calculations.

896 The protein-peptide docking resulted in 30 best poses of Receptor-ligand complexes.

897 The predicted poses are ranked based on the maximum number of occurrences of

898 that particular pose. Since there is no prior information about the binding pattern of

899 Nef with CD80/CD86, it is necessary to score each pose based on energy

900 calculations. The association of the protein-peptide complex is estimated by an

901 automated mechanism of Multi-Ligand Bimolecular Association with Energetics

902 (eMBrAcE) (MacroModel, version 9.6, Schrödinger, LLC, New York, NY, 2008). The

903 best identified Nef-CD80 binding pose analysed further for important amino acids

904 involved in the non-bonded interactions which is contributing for binding. In order to

905 validate the predicted binding mode, best binding small molecule **AP5** was docked

906 with the full-length Nef model. This was basically achieved by selection of a centroid

907 point from the predicted Nef-CD80 binding site using Glide docking protocol from

908 Schrodinger software. The top poses of the docked complexes were further

909 examined for the non-bonded interactions and best docked score.

910 **SAXS data collection and analysis**

911 SAXS-data of the apo HIV1-Nef was measured with the BIOSAXS-1000 small-angle

912 X-ray scattering with Kratky camera system, installed on a Rigaku microfocus X-ray

913 generator (1.5418 Å wavelength). The purified HIV1-Nef at 1, 3 and 5 mg/ml

914 concentrations were used with buffer containing 50 mM Tris/HCl, pH 7.5, 200 mM

915 NaCl in a sample volume of 60 µl inside a vacuum tight quartz capillary subjected X-

916 rays at 25 °C. The data was collected for 30 min and for each measurement a total of

917 six frames at 5 min intervals were recorded. Corresponding to each protein sample,

918 data were collected for a buffer under identical experimental conditions, providing a

919 background scattering curve. The data was then tested for possible radiation damage

920 by comparing the six data frames and no changes were observed. The scattering of

921 the buffer was subtracted from the scattering of the sample. All the data processing

922 steps were performed using the program package PRIMUS[47]. The experimental data

923 obtained for all protein samples were analyzed for aggregation using the Guinier

924 region. The forward scattering $I(0)$ and the radius of the gyration, R_g were computed

925 using the Guinier approximation assuming that at very small angles ($q<1.3/R_g$) the

926 intensity is represented as $I(q)= I(0)\exp(-(qR_g)2/3)$. These parameters were also

927   computed from the extended scattering patterns using the indirect transform package

928   GNOM, which provides the distance distribution function P(r) of the maximum particle

929   dimension, Dmax as well as the radius of gyration, Rg, qualitative particle motion was

930   inferred by plotting the scattering patterns in the normalized Kratky plot

931    $((qRg)2(I(q)/I(0))$ vs qRg). Ab initio low-resolution models of the proteins were built by

932   the program DAMMIF[48] considering low angle data ($q<2nm^{-1}$). Ten independent ab

933   initio reconstructions were performed for each protein and then averaged using

934   DAMAVER[49]. Superimposition between ab initio reconstruction and atomic model was

935   performed using the software SUPCOMB[50].

936   **Statistical Analysis:** Z factor was used for qualifying the plate and t-test was used

937   for determining the significant data. The plots were prepared using Graph Pad Prism

938   Ver6.0.

939

940

941 **Supplementary Information**

942 **Supplementary figure legends**

943 **Fig. S1**: **a)** Sequence of Subtype B and C with overlapping residues and important

944 residues highlighted (in red) **(b).** Sequence of full length CD80 and CD86, where the

945 20-mer cytoplasmic peptide used for screening assays are highlighted (in cyan) **(c)**

946 Schematic of ELISA procedure in microwell plate where the CD80 and CD86

947 peptides were immobilized. The Nef protein was incubated with the peptide and their

948 interaction was detected by anti-Nef antibody and secondary antibody with HRP. The

949 colorimetric signal was quantified with TMB reducing the HRP substrate

950 **Fig. S2:** Detailed chemical synthesis of the hits belongs to the AP, PA and BC

951 scaffolds. **Note: Details of Characterization of Synthesized compounds and**

952 **intermediates will be included in the full submission**.

953 **Fig. S3:** Regression graph showing correlation with replicate data R^2 values for hit

954 compounds in biochemical screen, where pIC_{50} is the negative log of IC_{50}

955 expressed in molar units.

956 **Fig. S4**: Graph shows cytotoxicity profile with treatment of compounds. RAJI cell line

957 was treated at the highest concentration of 100 µM for 24 h and the supernatant

958 collected was estimated for WST assay.

959 **Fig. S5**: FACS histogram shows surface staining of CD80 and CD86 with APC-

960 tagged specific CD80 or CD86 antibody. Colour representation: Unstained Cells (in

961 red), Isotype controls -IgG1k for CD80; IgG2b for CD86 (in blue dotted line), cells

962 with Vehicle control Chariot reagent showing CD80 or CD86 surface expression (in

963 orange), Protein delivered (in green). The reduction in CD80/CD86 levels are seen

964 with Nef protein after its delivery into RAJI cells in 2h incubation period. The surface

965 levels of CD80 did not change with the delivery of 100 μg of Ovalbumin and β-

966 lactoglobulin proteins with Chariot^{TM} reagent.

967 **Fig. S6: Schematic of the reterovirus used for infection assays.** Distribution of

968 regulatory elements in the HIV-1. (A) Schematic depiction of the HIV-1 genome

969 containing accessory *vpr*, *vpu*, and *nef* genes. (B) Schematic depiction of reteroviral

970 vector with Nef transgene. where Env protein used in this reterovirus is VsVg from

971 pMLV, and Vpr , Vif and Vpu are not present in this vector**.**

972 **Fig. S7: a)** SAXS-patterns of full length HIV1-Nef at three different concentrations 1,

973 3 and 5 mg/ml are shown. The Guinier plots at low angles appeared linear and

974 showed no aggregation (shown in inset) **(b)** The Rg, Dmax and molecular mass of

975 the full length HIV1-Nef suggest the progressive increase in the Rg, Dmax and

976 molecular mass values with increasing concentration of Nef. The deviation from a

977 typical bell-shaped profile depicts an inherent structural flexibility of Nef Protein **(c)**

978 The averaged ab initio model (surface representation) overlay with the crystal

979 structure of folded C-terminal core (cartoon representation).

980 **Fig. S8**: **a)** SDS-PAGE run with purified Nef proteins. Nef wildtype and mutants show

981 bands at ~29kDa **(b)** FPLC purification profile of Nef proteins purified (c) Western

982 blot showing Nef WT or mutant Nef protein delivered in RAJI cells post 5 h. Band

983 intensity of Nef^{W61A} protein reduced after 5 h when compared to 2 h incubation,

984 indicating degradation of protein.

985 **Supplementary tables:**

986 **Suppl. Table 1:** a) Table shows 20 compounds selected from screen showing IC$_{50}$s

987 in sub-micromolar ranges. Of these top 10 were chosen based on ease of

988 synthesis , efficacy and their cytotoxicity.

989   **Suppl. Table 2:** Table showing the SAXS derived parameters such as Guinier Rg,

990   Realspace Rg and Dmax for the full-length Nef in solution

991   **Suppl. Table. 3**: Table showing the residue information about the CD80 peptide

992   docked predicted sites on Nef from SiteMap program. The important residues

993   involved in protein-protein interactions are highlighted.

994

References

1. Tsibris, A. M. N. & Hirsch, M. S. MINIREVIEW Antiretroviral Therapy in the Clinic □. **84**, 5458–5464 (2010).

2. Gulick, R. M. & Flexner, C. Long-Acting HIV Drugs for Treatment and Prevention. (2019).

3. Kumar, A. & Herbein, G. The macrophage: a therapeutic target in HIV-1 infection. *Mol. Cell. Ther.* **2**, 10 (2014).

4. Baxter, J. *et al.* Global HIV-1 transmitted drug resistance in the INSIGHT Strategic Timing of AntiRetroviral Treatment (START) trial. *HIV Med.* **16**, 77–87 (2015).

5. Niessl, J. *et al.* Combination anti-HIV-1 antibody therapy is associated with increased virus-specific T cell immunity. *Nat. Med.* **26**, 222–227 (2020).

6. Pollara, J., Easterhoff, D. & Fouda, G. G. Lessons learned from human HIV vaccine trials. *Curr. Opin. HIV AIDS* **12**, 216–221 (2017).

7. Restouin, A. *et al.* Protein – protein interaction inhibition (2P2I) combining high throughput and virtual screening : Application to the HIV-1 Nef protein. **104**, (2007).

8. Flexner, C. Modern Human Immunodeficiency Virus Therapy : Progress and Prospects. **105**, 61–70 (2019).

9. Jäger, S. *et al.* Global landscape of HIV – human protein complexes. **481**, 365–370 (2013).

10. Arhel, N. J. & Kirchhoff, F. Implications of Nef: Host Cell Interactions in Viral Persistence and Progression to AIDS. in *HIV Interactions with Host Cell Proteins* (eds. Spearman, P. & Freed, E. O.) 147–175 (Springer Berlin Heidelberg, 2009). doi:10.1007/978-3-642-02175-6_8

11.   Peter, F. HIV nef: The mother of all evil? *Immunity* **9**, 433–437 (1998).

12.   Basmaciogullari, S. & Pizzato, M. The activity of Nef on HIV-1 infectivity. *Front. Microbiol.* **5**, 1–12 (2014).

13.   Rahim, M. M. A., Hanna, Z., Hu, C., Jolicoeur, P. & Chrobak, P. Adult AIDS-Like Disease in a Novel Inducible Human Immunodeficiency Virus Type 1 Nef Transgenic Mouse Model: CD4+ T-Cell Activation Is Nef Dependent and Can Occur in the Absence of Lymphophenia. *J. Virol.* **83**, 11830–11846 (2009).

14.   Greenway, A. L., Mills, J., Rhodes, D., Deacon, N. J. & McPhee, D. A. Serological detection of attenuated HIV-1 variants with nef gene deletions. *Aids* **12**, 555–561 (1998).

15.   Dyer, W. B. *et al.* Strong human immunodeficiency virus (HIV)-specific cytotoxic T-lymphocyte activity in Sydney Blood Bank Cohort patients infected with nef-defective HIV type 1. *J Virol* **73**, 436–443 (1999).

16.   Birch, M. R. *et al.* An examination of signs of disease progression in survivors of the Sydney Blood Bank Cohort (SBBC). *J. Clin. Virol.* **22**, 263–270 (2001).

17.   Brambilla, A. *et al.* Defective nef alleles in a cohort of hemophiliacs with progressing and nonprogressing HIV-1 infection. *Virology* **259**, 349–368 (1999).

18.   Trible, R. P. *et al.* Allosteric Loss-of-function Mutations in HIV-1 Nef from a Long-term Non-progressor. *J. Mol. Biol.* **374**, 121–129 (2007).

19.   Das, S. R. & Jameel, S. Biology of the HIV Nef protein. *Indian J. Med. Res.* **121**, 315–332 (2005).

20.   Swingler, S., Brichacek, B., Jacque, J. & Ulich, C. HIV-1 Nef intersects the macrophage CD40L signalling pathway to promote resting-cell infection. **424**, 213–219 (2003).

21. Pereira, E. A. & daSilva, L. L. P. HIV-1 Nef: Taking Control of Protein Trafficking. *Traffic* **17**, 976–996 (2016).

22. Roeth, J. F. & Collins, K. L. Human Immunodeficiency Virus Type 1 Nef : Adapting to Intracellular Trafficking Pathways. **70**, 548–563 (2006).

23. Landi, A., Iannucci, V., Van Nuffel, A., Meuwissen, P. & Verhasselt, B. One Protein to Rule them All: Modulation of Cell Surface Receptors and Molecules by HIV Nef. *Curr. HIV Res.* **9**, 496–504 (2011).

24. Chaudhry, A. *et al.* The Nef Protein of HIV-1 Induces Loss of Cell Surface Costimulatory Molecules CD80 and CD86 in APCs. *J. Immunol.* **175**, 4566–4574 (2005).

25. Chaudhry, A. *et al.* A Two-Pronged Mechanism for HIV-1 Nef-Mediated Endocytosis of Immune Costimulatory Molecules CD80 and CD86. *Cell Host Microbe* **1**, 37–49 (2007).

26. Chaudhry, A. *et al.* HIV-1 Nef promotes endocytosis of cell surface MHC class II molecules via a constitutive pathway. *J. Immunol.* **183**, 7611–7611 (2009).

27. Seidel, S. A. I. *et al.* Microscale thermophoresis quantifies biomolecular interactions under previously challenging conditions. *Methods* **59**, 301–315 (2013).

28. Venzke, S., Michel, N., Allespach, I., Fackler, O. T. & Keppler, O. T. Expression of Nef Downregulates CXCR4, the Major Coreceptor of Human Immunodeficiency Virus, from the Surfaces of Target Cells and Thereby Enhances Resistance to Superinfection. *J. Virol.* **80**, 11141–11152 (2006).

29. Snanoudj, R. *et al.* The blockade of T-cell co-stimulation as a therapeutic stratagem for immunosuppression: Focus on belatacept. *Biol. Targets Ther.* **1**, 203–213 (2007).

30. Geyer, M., Munte, C. E., Schorr, J., Kellner, R. & Kalbitzer, H. R. Structure of the Anchor-Domain of Myristoylated and Non-myristoylated HIV-1 Nef Protein. **4**, (1999).

31. Barnham, K. J., Monks, S. A., Hinds, M. G., Azad, A. A. & Norton, R. S. Solution Structure of a Polypeptide from the N Terminus of the HIV Protein Nef. **2960**, 5970–5980 (1997).

32. Horenkamp, F. A. *et al.* Conformation of the Dileucine-Based Sorting Motif in HIV-1 Nef Revealed by Intermolecular Domain Assembly. 867–877 (2011). doi:10.1111/j.1600-0854.2011.01205.x

33. Geyer, M. & Peterlin, B. M. Domain assembly, surface accessibility and sequence conservation in full length HIV-1 Nef. *FEBS Lett.* **496**, 91–95 (2001).

34. Chi-Hon, L., Saksela, K., Mirza, U. A., Chait, B. T. & Kuriyan, J. Crystal structure of the conserved core of HIV-1 Nef complexed with a Src family SH3 domain. *Cell* **85**, 931–942 (1996).

35. Dikeakos, J. D. *et al.* An interdomain binding site on HIV-1 Nef interacts with PACS-1 and PACS-2 on endosomes to down-regulate MHC-I. (2011). doi:10.1091/mbc.E11-11-0928

36. Viruses, I., Lindwasser, O. W., Chaudhuri, R. & Bonifacino, J. S. Mechanisms of CD4 Downregulation by the Nef and Vpu Proteins of Primate Mechanisms of CD4 Downregulation by the Nef and Vpu Proteins of Primate Immunodeficiency Viruses. (2007). doi:10.2174/156652407780059177

37. Swigut, T., Shohdy, N. & Skowronski, J. Mechanism for down-regulation of CD28 by Nef. *EMBO J.* **20**, 1593–1604 (2001).

38. Pawlak, E. N. & Dikeakos, J. D. Biochimica et Biophysica Acta HIV-1 Nef : a master manipulator of the membrane traf fi cking machinery mediating immune

evasion MHC-I Downregulation By Nef MHC-I Secretory Pathway Transport PACS-2 MHC-I. *BBA - Gen. Subj.* **1850**, 733–741 (2015).

39. Buffalo, C. Z., Iwamoto, Y., Hurley, J. H. & Ren, X. crossm. 1–18 (2019).

40. Khan, N., Gowthaman, U., Pahari, S. & Agrewala, J. N. Manipulation of costimulatory molecules by intracellular pathogens: Veni, Vidi, Vici!! *PLoS Pathog.* **8**, (2012).

41. Singh, R. K., Lau, D., Noviello, C. M., Ghosh, P. & Guatelli, J. C. An MHC-I cytoplasmic domain/HIV-1 nef fusion protein binds directly to the µ subunit of the AP-1 endosomal coat complex. *PLoS One* **4**, 1–7 (2009).

42. Subauste, C. S., de Waal Malefyt, R. & Fuh, F. Role of CD80 (B7.1) and CD86 (B7.2) in the immune response to an intracellular pathogen. *J. Immunol.* **160**, 1831–40 (1998).

43. Köchli, C. *et al.* CD80 and CD86 costimulatory molecules on circulating T cells of HIV infected individuals. *Immunol. Lett.* **65**, 197–201 (1999).

44. Ahmad, N. NIH Public Access. *Life Sci* **88**, 980–986 (2011).

45. Vanhove, B. Co-stimulatory blockade of the CD28 / CD80-86 / CTLA-4 balance in transplantation : impact on memory T cells ? **6**, 1–11 (2015).

46. Wishart, D. NMR Spectroscopy and Protein Structure Determination: Applications to Drug Discovery and Development. *Curr. Pharm. Biotechnol.* **6**, 105–120 (2005).

47. Konarev, P. V *et al.* PRIMUS : a Windows PC-based system for small-angle scattering data analysis PRIMUS : a Windows PC-based system for small-angle scattering data analysis. 1277–1282 (2003).

48. Franke, D. & Svergun, D. I. DAMMIF , a program for rapid ab-initio shape determination in small-angle scattering. 342–346 (2009).

doi:10.1107/S0021889809000338

49. Volkov, V. V & Svergun, D. I. small-angle scattering. 860–864 (2003).

50. Kozin, M. B. & Svergun, D. I. Automated matching of high- and low-resolution
     structural models research papers Automated matching of high- and low-
     resolution structural models. 33–41 (2001).

Main Figures

Graphical Abstract

Fig. 1

a

CD80 receptor / CD86 receptor

1-242 a.a — Extracellular receptor — 1-247 a.a

243-263 a.a — Transmembrane — 248-268 a.a

Cytoplamic tails

262-288 a.a / 269-329 a.a

CD80 20-mer tail peptide 269-288 a.a (PRCRERRRNERLRRESVRPV)

CD86 20-mer tail peptide 267-286 a.a (LWKWKKKKRPRNSYKCGTNT)

b Nef with CD80

$kD = 27\mu M$

x axis: Concentration (nM); y axis: ΔFnorm (%)

c Nef with CD86

$kD = 112nM$

x axis: Concentration (nM); y axis: ΔFnorm (%)

d

y axis: OD at 450nm

Blank, CD80, CD86, CD74, CD80, CD86, CD74

Nef: −, −, −, −, +, +, +

e y axis: % NPI (CD80); x axis: Compounds; Actives

f y axis: % NPI (CD86); x axis: Compounds; Actives

g

Total 1061 library molecules → Primary Screening through ELISA → 34 Active Hits → Belongs to 9 scaffold

Aminopyrimidine(AP) (5 molecules); Phenoxyacetamide(PA) (10 molecules); Benzothiazolpyrazolone(BP) (1 molecule); Benzimidazole(BI) (1 molecule); Biaryl(heteroaryl) carbamate(BC) (10 molecules); Benzofuranamide(BA) (3 molecules); Benzothiazole hydrazone(BH) (2 molecules); Quinoline phenothiazine(QP) (1 molecule); Butyrolactum(BL) (1 molecule)

h

AP5 $IC_{50} = 5$ nM

x axis: Log Conc(µM); y axis: NPI

Amino Pyrimidine-5 (AP-5)
MW: 419
CLogP: 4.3
TPSA: 90.4
NRB: 6
IC50= 5nM

AP-5
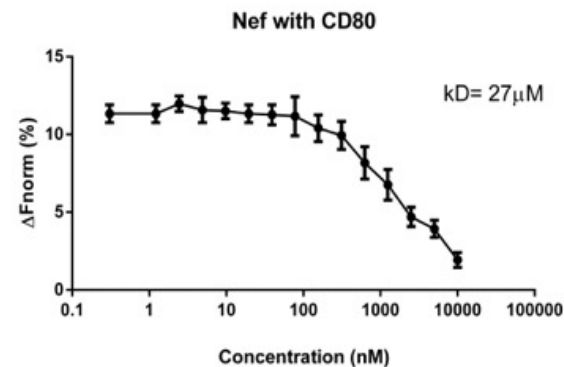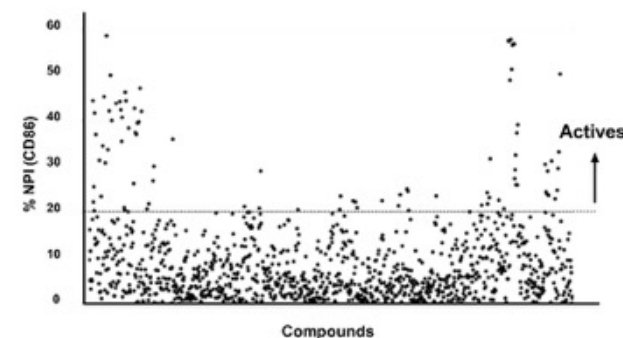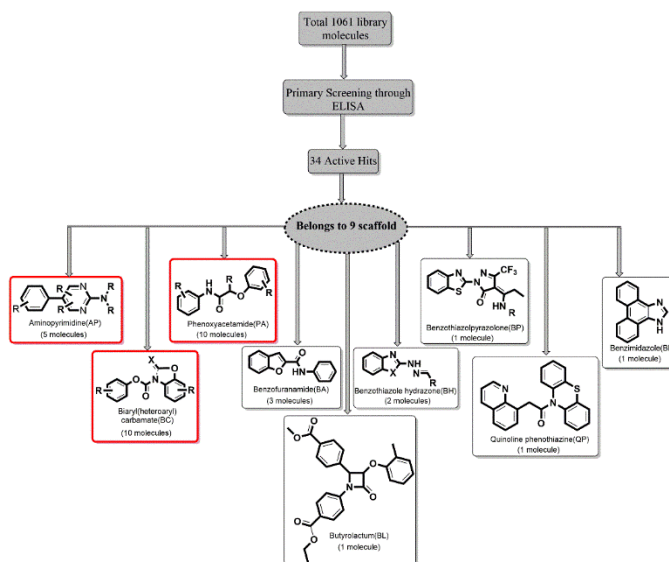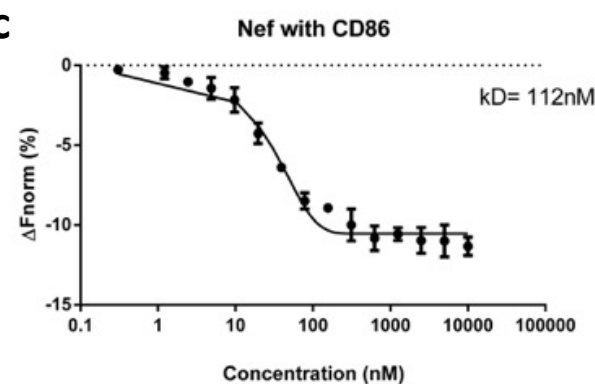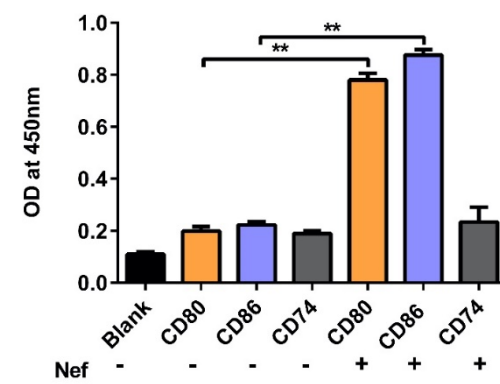
Fig. 1 Nef directly interacts with the cytoplasmic tail peptides of CD80/86. a) Illustration shows the CD80 and CD86 receptors with their extracellular, transmembrane and cytosolic tail region marked. The 20-mer peptide region of CD80 (PRCRERRRNERLRRESVRPV, 269 to 288 a.a) and CD86 (LWKWKKKKRPRNSYKCGTNT, 267-286 a.a) is highlighted within the cytoplasmic tail domain (b) Graph shows direct binding of Nef to CD80 as measured by Microscale scale thermophoresis (MST). CD80 peptide was titrated from 950 µM in 2-fold dilutions upto 16 points against a fixed Nef concentration (35 nM) in the final reaction volume. A curve with upper saturation with kD=27 µM was obtained; x axis= peptide concentration (nM) and y axis= percentage normalized fluorescence (ΔFnorm); Plots represent the mean ± SD (error bars) from three independent experiments.(c) Similarly, CD86 peptide was titrated from 10 µM with a 2-fold serial dilution upto 16 points against a fixed Nef concentration (35 nM). A sigmoidal curve with kD=112 nM, showing higher affinity as compared to CD80. (d) Graph shows ELISA assay where change in OD is observed when the immobilized CD80 and CD86 cytosolic peptides binds to Nef. The OD measurement was done at 450nm. CD74, a negative peptide control shows minimal OD value (e) Graph shows Normalized Percentage Index (NPI) on a normal distribution curve for statistical significance of active compounds across qualified plates showing CD80 actives. X axis= the number of compounds screened in ELISA assay; y axis= normalized percentage Inhibition of compounds; of Z-factor>0.5 analysis was used to qualify the plates. Compounds with NPI>30% for CD80 was considered as hits (f) Similarly, NPI normal distribution curve for CD86 with Cutoff percentage for CD86 NPI>20% was considered as hits (g) Scheme shows the hits belonging to 9 scaffolds that were identified in the primary screen (h) Dose response curve of a hit compound from "AP" scaffold; x axis= log concentration of compounds; y axis= Normalized percentage Inhibition, (inset) Structure of AP5 compound and its molecular properties
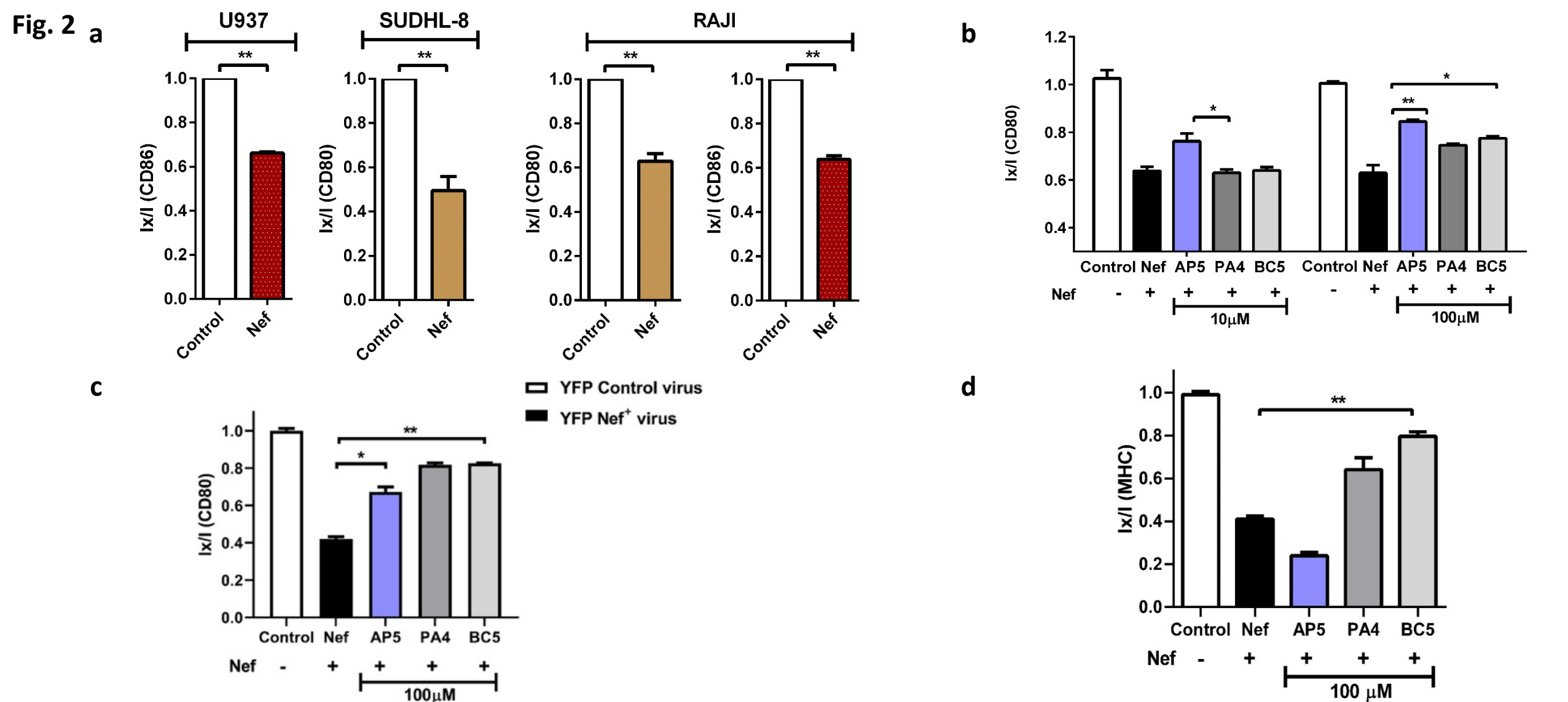
Fig. 2: Cell based assay screening of active compounds from ELISA. (a) Nef mediated down-regulation of surface CD80 or CD86 in 3 different cell lines as indicated. FACS data showing the normalized surface levels of CD80; I_x/I (y axis) where I_x is the average fluorescence intensity in the indicated condition (from a triplicate) and I is the Median of normalized negative control (No Nef control) (b) FACS data shows restoration of CD80 receptors in RAJI cell line after pre-treatment with 3 representative compounds **AP5, PA4 and BC5** at 10 and 100 µM for 24 h and analysis after 2 h post Nef protein delivery (c) RAJI cell line was infected with viral particles (Nef-YFP and YFP alone control cells) in viral infection assay and surface CD80 receptors with compounds were measured by flow cytometry (d) Effects of inhibitors on Nef-MHC-I interactions. RAJI cells were treated with compounds at 100 µM and then stained with anti-MHC-I antibody. MHC-I was detected by flow cytometry and shown as I_x/I plots. Compound **AP5** shows no restoration of MHC-I indicating its specificity for the Nef-CD80 interface.
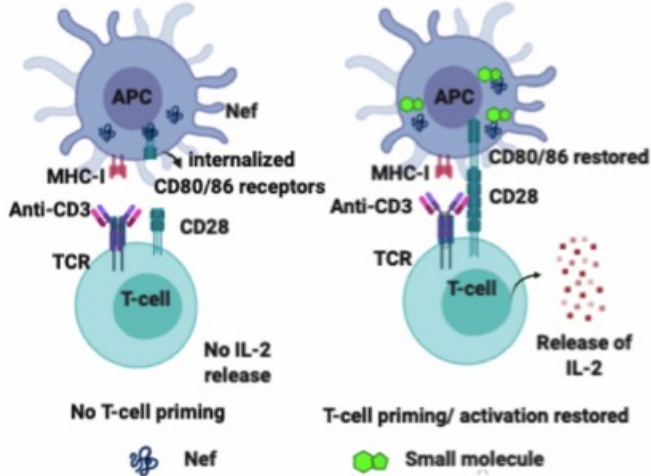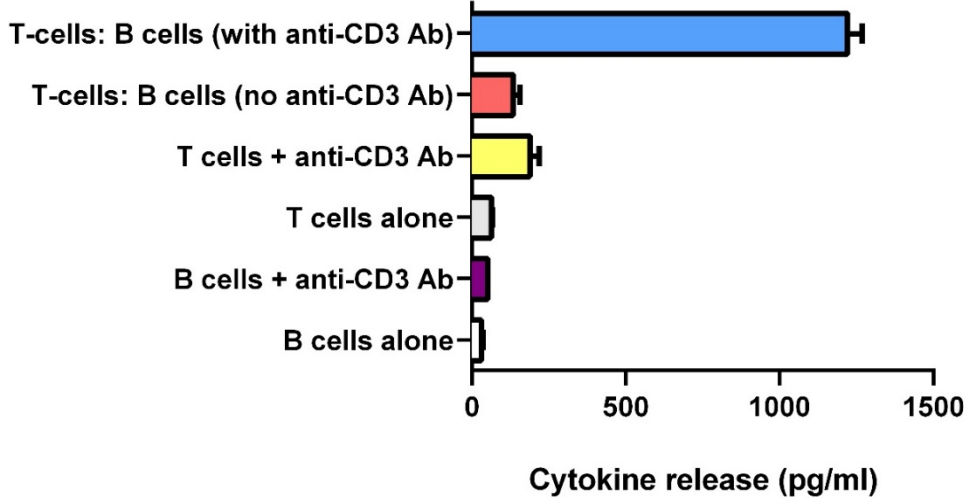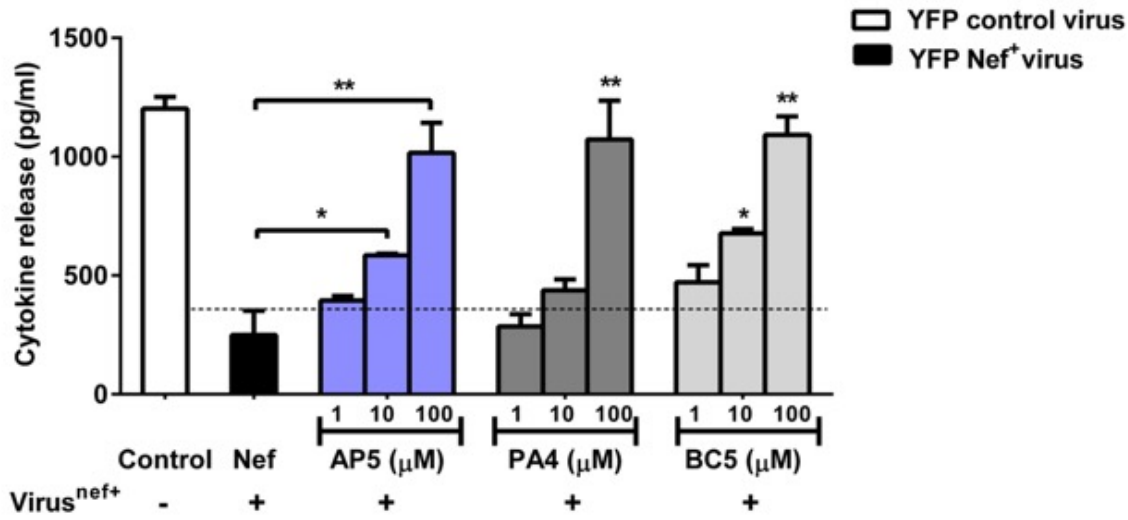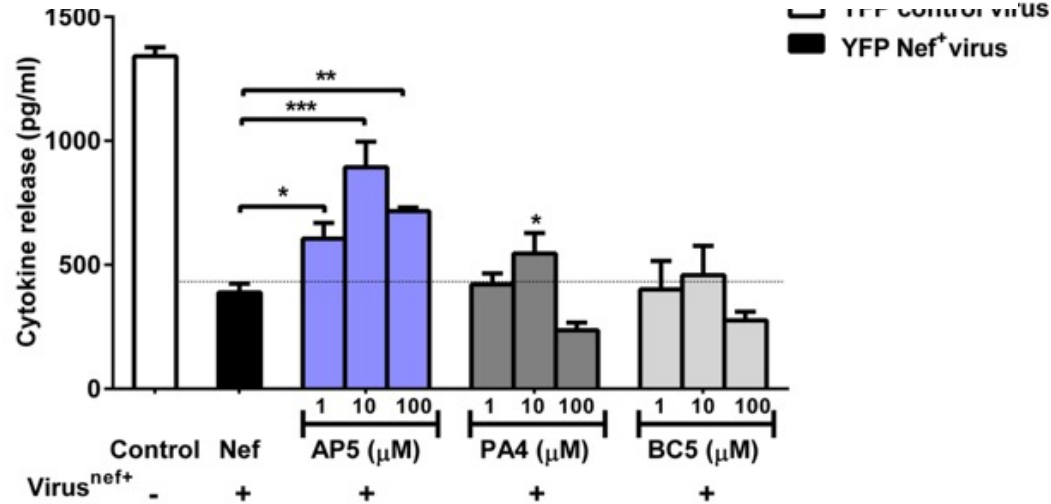
Fig. 3: Restoration of functional T-cell activation in a viral infection assay (a) Schematic of a functional assay for screening of compounds that disrupt Nef-CD80/86 interactions in a virally-infected cell. Functional T-Cell activation is based on APC-T cell co-cultures. The APC has CD80/86 and concurrent presence of anti-CD3 antibody promotes T-cell activation (as measured via IL-2) in co-cultured T-cells (b) Graph shows cytokine release in functional T-cell activation assay where antigen presenting cell RAJI (B-cells) and Jurkat-cells (T cells) were co-cultured as indicated (with/without anti-CD3 antibody); T-cells alone, B-cells alone controls do not show measurable IL-2 release. (c) Graph shows quantification of cytokine (IL-2) released after T-cells and B-cells co-culture for 3 h; here B-cells were pretreated with the indicated concentrations (1, 10, 100 μM) of compounds for 24 h followed by viral infection for 96 h (d) Graph shows quantification of cytokine (IL-2) released after T-cells and B-cells co-culture for 3 h; here B-cells were first infected with virus for 96h and then treated with compounds at 1, 10, 100 μM for 24 h. IL-2 release (pg/ml) was determined by ELISA by plotting against an IL-2 standard curve. Note: viral infection reduces IL-2 release, and all 3 compounds showed a dose dependent restoration of IL-2 release. **AP5** showed IL-2 release at 1 μM.
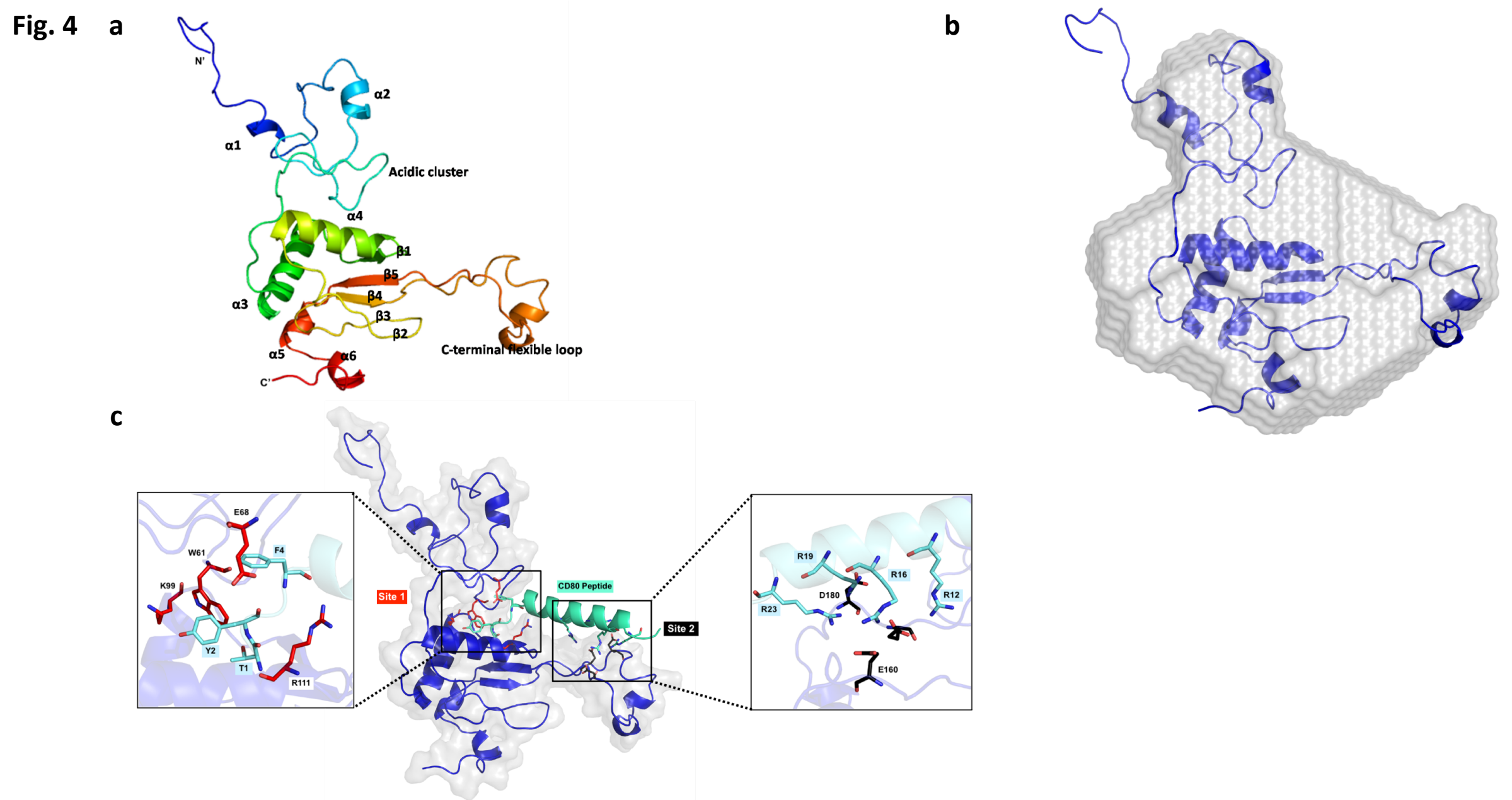
Fig. 4: Modelling of Nef with multi-template computational approach (a) Cartoon representation of the predicted structure of Nef shows flexible N-terminal region and well-conserved core domain, colored in accordance with their position (N-terminal in blue to C-terminal in red) with respective α-helices and β-sheets as indicated. (b) The *ab initio* shape of the solution structure of the Nef (blue color) from the SAXS data (grey surface) fits well with the computational model (cartoon representation) (c) Surface representation of HIV-1 Nef is depicted with the best CD80 binding pose. CD80 peptide in a docked pose (cyan color) in Nef obtained using SiteMap program. The inset shows the important residues of Nef involved in interaction with CD80 at Sites 1 and 2.
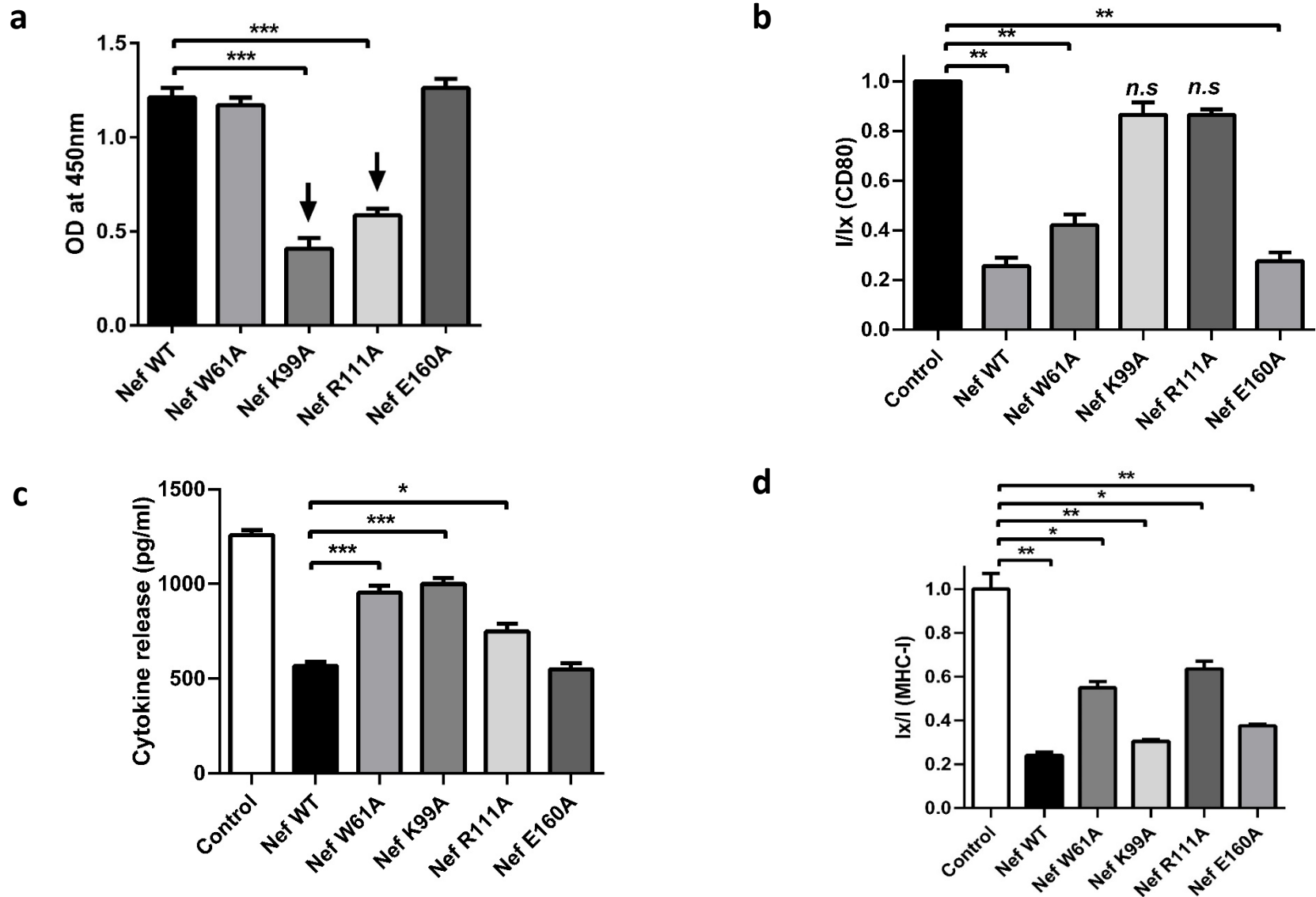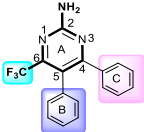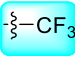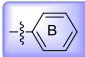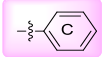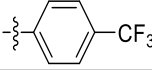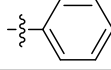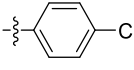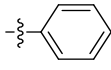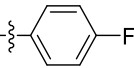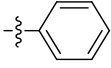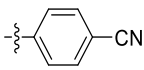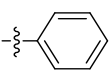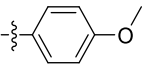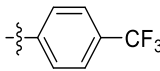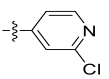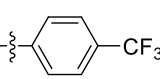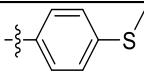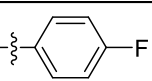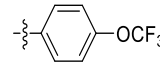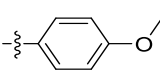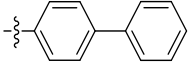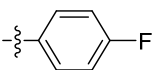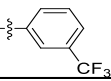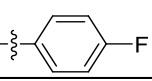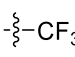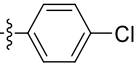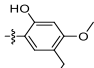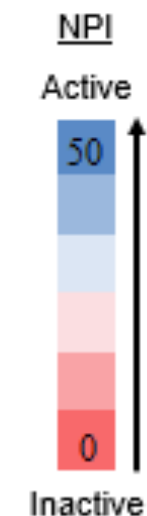
Fig. 5: Evaluation of interaction between CD80 and Nef mutants in biochemical and cell-based assays (a) Graph shows colorimetric signal of immobilized CD80 cytosolic peptide upon binding to Nef^{WT} or Nef mutants as measured by ELISA at OD450nm. Two mutants Nef^{K99A} and Nef^{R111A} showed reduced affinity to CD80 peptide (b) Graph shows FACS data of surface levels of CD80 receptors in RAJI cell line after delivery of Nef^{WT} or Nef mutant protein delivery . No significant down regulation seen with mutants Nef^{K99A} and Nef^{R111A} (c) Graph shows the levels cytokine (IL-2) released in supernatants of cells in the co-culture functional T-cell activation assay after delivery of the Nef mutants as compared to the wild type Nef protein. (d) Graph shows FACS data of MHC-1 levels after delivery with Nef^{WT}and mutants. Nef^{WT} or mutants were delivered into RAJI cells using Chariot^{TM} delivery reagent. MHC-I was detected by flow cytometry and shown as Ix/I plots.
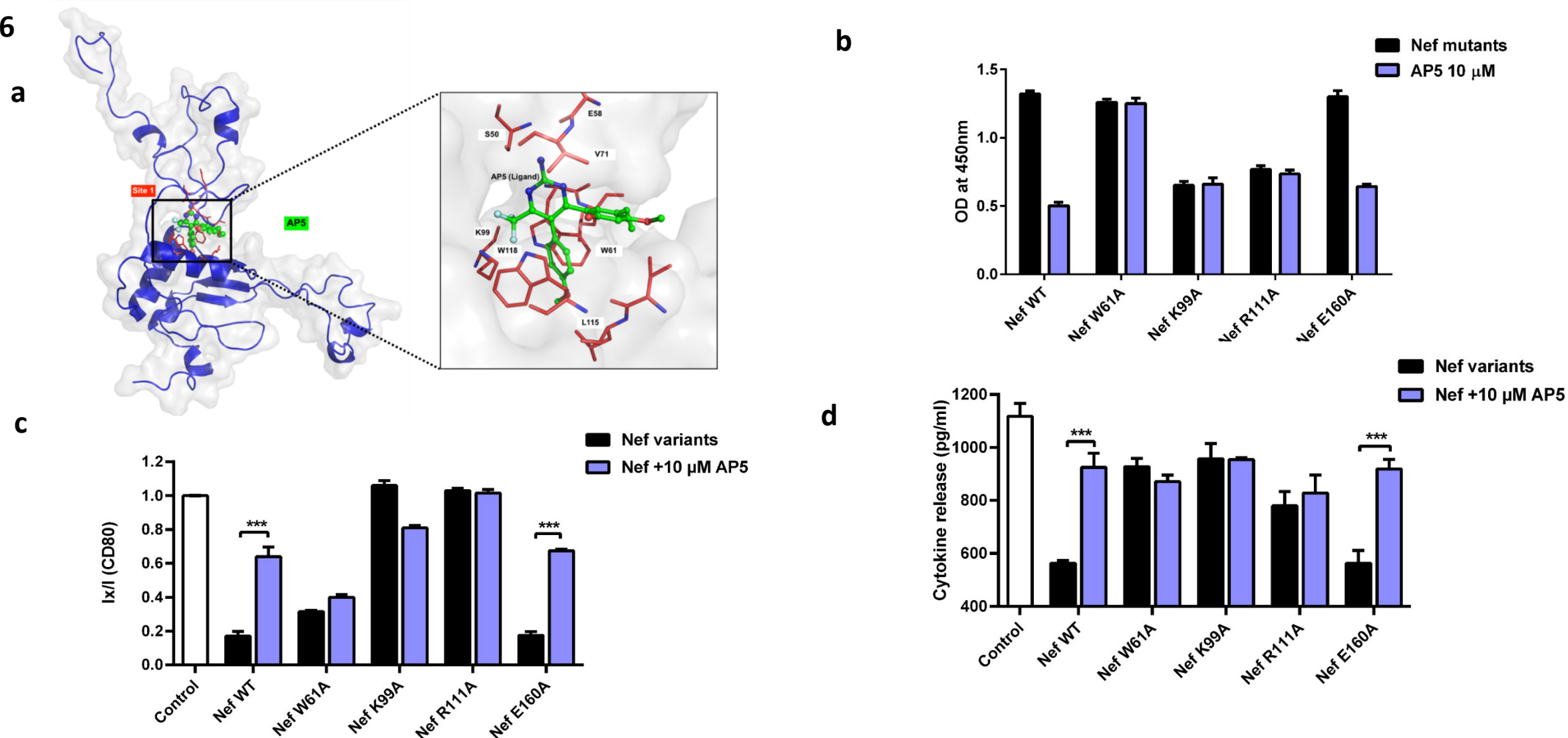
Fig. 6: Structural and functional evaluation of the interaction between Nef and AP5 (a) Surface representation of HIV-1 Nef depicting **AP5** ligand (green color) binding. The binding site of **AP5** molecule overlaps with the CD80 binding site (Site-1). The inset shows the important residues for the interaction between AP5 and Nef. The non-polar residues such as W_{61}, L_{91}, I_{109} and L_{115} contribute to hydrophobic interactions with CF_3. **AP5** ligand docking studies shows that the binding interactions occurs between the α4 and α5 helices along with few residues such as W_{61}, E_{65} and R_{111} which are crucial for **AP5**-Nef interaction (b) Graph shows colorimetric signal of immobilized CD80 cytosolic peptide upon binding to Nef^{WT} or Nef mutants in the presence /absence of 10 μM AP5 as measured by ELISA at OD450 nm. (c) Graph shows surface levels of CD80 receptors in RAJI cell line after the delivery of Nef^{WT} or Nef mutant protein delivery as measured by FACS in the presence /absence of 10 μM AP5. Nef^{W61A}, Nef^{K99A} and Nef^{R111} did not show any further change in CD80 levels with **AP5** addition. (d) Graph shows cytokine (IL-2) release in supernatants after the co-culture T-cell activation assay. RAJI cells were pre-treated with 10 μM AP5 for 1 h and then the cells were delivered with Nef mutants or wild type Nef protein for 2 h before co-culture with Jurkat T-cells for 3 h. The IL-2 levels remain unchanged with and without addition of **AP5** compound in all three mutants Nef^{W61A}, Nef^{K99A} and Nef^{R111}. Reduction in IL-2 seen with mutant Nef^{E160A} comparable to Nef^{WT}.

Fig. 7: **SAR and Hit refinement with AP5 as a template** (a) Scheme shows Medicinal chemistry approach for hit refinement of **AP5** showing two series of compounds (b) Summary of SAR strategy to design compounds similar to **AP5 structure** with modifications made on rings A, B and C as indicated. The synthesized molecules were evaluated for their effect on Nef-CD80/CD86 inhibition (c) Heat map table showing SAR with synthesized compounds. The various substitutions in rings A, B and C are indicated as well as their activity in the ELISA and cell-based assays